

Genome-scale metabolic modelling of responses to polymyxins in *Pseudomonas aeruginosa* --Manuscript Draft--

Manuscript Number:	GIGA-D-17-00272R1	
Full Title:	Genome-scale metabolic modelling of responses to polymyxins in <i>Pseudomonas aeruginosa</i>	
Article Type:	Research	
Funding Information:	Monash University (Major Interdisciplinary Research Grant)	Prof Jian Li
	National Health and Medical Research Council (APP1127948)	Prof Jian Li
	National Institute of Allergy and Infectious Diseases (R01 AI111965)	Prof Jian Li
	National Health and Medical Research Council (APP1086825)	Dr Tony Velkov
	National Health and Medical Research Council (APP1063069)	Prof Jian Li
	Australian Research Council (FL130100038)	Prof Trevor Lithgow
Abstract:	<p>Background: <i>Pseudomonas aeruginosa</i> often causes multidrug-resistant infections in immunocompromised patients and polymyxins are often used as the last-line therapy. Alarming, resistance to polymyxins has been increasingly reported worldwide recently. To rescue this last-resort class of antibiotics, it is necessary to systematically understand how <i>P. aeruginosa</i> alters its metabolism in response to polymyxin treatment, thereby facilitating the development of effective therapies. To this end, a genome-scale metabolic model (GSMM) was employed to analyse bacterial metabolic changes at the systems level.</p> <p>Findings: A high-quality GSMM iPAO1 was constructed for <i>P. aeruginosa</i> PAO1 for antimicrobial pharmacological research. Model iPAO1 encompasses an additional periplasmic compartment and contains 3,022 metabolites, 4,265 reactions and 1,458 genes in total. Growth prediction on 190 carbon and 95 nitrogen sources achieved an accuracy of 89.1%, outperforming all reported <i>P. aeruginosa</i> models. Notably, prediction of the essential genes for growth achieved a high accuracy of 87.9%. Metabolic simulation showed that lipid A modifications associated with polymyxin resistance exert a limited impact on bacterial growth and metabolism, but remarkably change the physiochemical properties of the outer membrane. Modelling with transcriptomics constraints revealed a broad range of metabolic responses to polymyxin treatment, including reduced biomass synthesis, upregulated amino acids catabolism, induced flux through the tricarboxylic acid cycle, and increased redox turnover.</p> <p>Conclusions: Overall, iPAO1 represents the most comprehensive GSMM constructed to date for <i>Pseudomonas</i>. It provides a powerful systems pharmacology platform for the elucidation of complex killing mechanisms of antibiotics.</p>	
Corresponding Author:	Jian Li AUSTRALIA	
Corresponding Author Secondary Information:		
Corresponding Author's Institution:		
Corresponding Author's Secondary Institution:		
First Author:	Yan Zhu	

First Author Secondary Information:	
Order of Authors:	Yan Zhu
	Tobias Czauderna
	Jinxin Zhao
	Matthias Klapperstueck
	Mohd Hafidz Mahamad Maifiah
	Mei-Ling Han
	Jing Lu
	Björn Sommer
	Tony Velkov
	Trevor Lithgow
	Jiangning Song
	Falk Schreiber
	Jian Li
Order of Authors Secondary Information:	
Response to Reviewers:	<p>Dr Laurie Goodman Editor-in-Chief GigaScience</p> <p>Dear Dr Goodman, RE: Manuscript ID: GIGA-D-17-00272: "Genome-scale metabolic modelling of responses to polymyxins in Pseudomonas aeruginosa"</p> <p>Thank you for the opportunity to revise our manuscript. Please find below a point-by-point response to the reviewers' comments. All major changes have been highlighted in yellow in the 'marked' version of the revised manuscript.</p> <p>The raw data have been submitted to Sequence Read Archive (SRA) and MetaboLights databases and will be made publicly available hopefully by 31 Jan, 2018. We look forward to your correspondence and thank you very much.</p> <p>Best regards,</p> <p>Jian Li Falk Schreiber</p> <p>Monash Biomedicine Discovery Institute, Department of Microbiology, Faculty of Medicine, Nursing and Health Sciences, Monash University, Melbourne 3800, Australia</p> <p>Department of Computer and Information Science, University of Konstanz, Konstanz 78457, Germany</p> <p>Reviewer #1:</p> <p>1. Introduction section. I would specify that the specific approach of applying gene expression constraints to obtain condition-specific GEMs have been previously used for other MDR bacteria (e.g. A. baumannii doi:10.1038/s41598-017-03416-2).</p> <p>Response: The manuscript has been revised accordingly (Pages 3-4, Lines 74-77).</p> <p>2. Lines 217-218: I would remove the sentence "Therefore, iPAO1 is a well-defined, metabolism-dedicated model.", in that it is included in the definition of "metabolic reconstruction". The presence of genes associated to non-metabolic COG categories is, in my opinion, due to the presence of misannotated (for what concerns the COG</p>

categories) genes. Honestly, I wouldn't use the distribution of such categories as a measure of a model goodness, especially considering that some genes can be associated to multiple categories. All the other comparisons the authors made already highlighted how this reconstruction is the best one.

Response: The sentence was removed in the revised manuscript as suggested (Page 9, Line 221).

3. Lines 253-258: "this is possibly due to the incorporation of new genes (30.5% increase compared to Opt208964; 27.2% increase compared to iPae1146) whose metabolic functions were previously misannotated." This is not clear... do the authors mean that the addition of new genes brought alternative routes to bypass previously essential gene deletion? This should be rephrased, and, if possible, the proposed explanation should be tested.

Response: The sentence was rephrased as suggested. In the revised manuscript an example was provided to delineate that incorporating isozymes altered previous essentiality prediction results. Please refer Page 11, Lines 256-264 in the revised manuscript.

4. Section "Elucidating the mechanisms of metabolic responses to polymyxin treatment":

In this section the authors use the previously presented model to describe the changes at a systems level of the metabolism in presence of polymyxin treatment. I have two issues concerning this section: The way the authors computed the flux distribution in presence of antibiotics. Given the non-optimal state of such condition, I feel that MOMA is more appropriate. I suggest the authors to test this and compare the results with the current ones.

Response: We respectfully disagree with the reviewer. Minimisation Of Metabolic Adjustment (MOMA) was developed to predict the metabolic flux redistributions in gene knockout mutants. MOMA hypothesises that metabolism of the mutant tends to approximate the wild-type (Segre et al., 2002, Proc Natl Acad Sci. 99(23):15112-7), which is distinct from the antibiotic treatment scenario. For instance, our metabolomics data have demonstrated that polymyxin treatment caused dramatic metabolic changes in bacteria (e.g. Maifiah et al., 2017, Sci Rep, 7: 45527). Therefore, metabolic fluxes with and without antibiotic treatment should not be calculated with MOMA, but FBA (see e.g. Colijn et al., 2009, PLoS Comput Biol, 5(8): e10004). Please refer Pages 17, Lines 414-420 in our revised manuscript.

5. Although a description of the systemic changes induced by antibiotics is important, I think that the authors are missing an important point, that is the condition-specific essential genes. In my opinion this is very important and interesting, also considering that a selling point of the manuscript is that "iPAO1 offers an in silico platform for precision antimicrobial pharmacology therapy".

Response: We appreciate reviewer's suggestion. The methods and results on the condition-specific essential genes were included in the revised manuscript (Page 23, Lines 552-555; Page 11, Lines 264-269).

Reviewer #2:

1. On page 13 line 260 in the section on lipid A modification the authors mention changes in fluxes. They state that fluxes were calculated using FBA. However, in the Methods section I see that the authors used sampling to explore the solution space. The authors must use sampling to compare fluxes between conditions. If the author's used sampling here to the authors must specify so in the main text.

Response: We employed sampling in our original study and have specified the sampling methods in the revised manuscript as suggested. Please refer Page 12, Lines 274, 286-287.

2. Page 14 line 286 - the authors must state how the RNAseq was used to constrain the model. They mention it in the Discussion section (E-FLUX method). However, this must be stated in the Results section as well.

	<p>Response: E-Flux method was employed to constrain the model with the RNAseq data, which has been specified in the Methods (Pages 24-25, Lines 586-592) and Results sections as suggested (Page 13, Line 302).</p> <p>3. Page 14 line 295 - I have a major question about how the authors simulate for growth in CAMHB media? This is an undefined media type and in the Methods section they describe that they set the uptake rates to 1 mmol*gDW*hr⁻¹ for major carbon sources. The authors must explain why this uptake rate is justified. Did the authors perform any sensitivity analysis on these uptake rates? It's very reasonable to assume that changes in these rates would dramatically affect the fluxes described by the authors in this section. Some justification and or sensitivity analysis must be added here to explain the validity of these uptake rates for growth in this condition.</p> <p>Response: Previous measurements showed that <i>P. aeruginosa</i> cells uptake amino acids at a rate ranging from 0.26 to 1.44 mmol·gDW⁻¹·h⁻¹ (J Bacteriol, 105(3): 1039-46; J Bacteriol, 152(2): 636-42). The import of CAMHB ingredients was thus constrained to 1 mmol·gDW⁻¹·h⁻¹ without loss of generality. Sensitivity analysis was conducted as suggested (Methods section, Page 25, Lines 592-597 and 600-602) and the results showed that the changes in nutrient uptake bounds did not dramatically affect the key metabolic fluxes. Our sensitivity analysis results have been provided in the Results section (Page 13, Lines 304-305), Additional File 1 and Figure S1.</p> <p>4. Page 15 line 303 - the authors must state what the "control" condition is. Is this compared to PAO1 growing in CAMHB without polymyxin treatment? Or compared to growth on a different media type, i.e. M9 minimal media + glucose?</p> <p>Response: The control condition was specified in the revised manuscript as suggested (Page 13 Line 321).</p> <p>5. The authors state that their model is "the most comprehensive for a gram-negative organism to date". On what basis is this claim made? We would recommend tempering this statement or perhaps limiting it to <i>Pseudomonas</i> models.</p> <p>Response: The statement was limited to <i>Pseudomonas</i> and was modified in the revised manuscript (Page 2, Line 46; Page 4, Line 98; Page 20, Line 472).</p>
Additional Information:	
Question	Response
Are you submitting this manuscript to a special series or article collection?	No
<p>Experimental design and statistics</p> <p>Full details of the experimental design and statistical methods used should be given in the Methods section, as detailed in our Minimum Standards Reporting Checklist. Information essential to interpreting the data presented should be made available in the figure legends.</p> <p>Have you included all the information requested in your manuscript?</p>	Yes
Resources	Yes
A description of all resources used,	

<p>including antibodies, cell lines, animals and software tools, with enough information to allow them to be uniquely identified, should be included in the Methods section. Authors are strongly encouraged to cite Research Resource Identifiers (RRIDs) for antibodies, model organisms and tools, where possible.</p> <p>Have you included the information requested as detailed in our Minimum Standards Reporting Checklist?</p>	
<p>Availability of data and materials</p> <p>All datasets and code on which the conclusions of the paper rely must be either included in your submission or deposited in publicly available repositories (where available and ethically appropriate), referencing such data using a unique identifier in the references and in the “Availability of Data and Materials” section of your manuscript.</p> <p>Have you have met the above requirement as detailed in our Minimum Standards Reporting Checklist?</p>	<p>Yes</p>

1 **Genome-scale metabolic modelling of responses to polymyxins in *Pseudomonas***
2 ***aeruginosa***

3 Yan Zhu¹, Tobias Czauderna², Jinxin Zhao¹, Matthias Klapperstueck², Mohd Hafidz
4 Mahamad Maifiah³, Mei-Ling Han³, Jing Lu⁴, Björn Sommer⁵, Tony Velkov⁶, Trevor
5 Lithgow¹, Jiangning Song¹, Falk Schreiber^{2,5*}, Jian Li^{1*}

6 ¹Monash Biomedicine Discovery Institute, Department of Microbiology, Faculty of Medicine,
7 Nursing and Health Sciences, Monash University, Melbourne 3800, Australia; ²Faculty of
8 Information Technology, Monash University, Melbourne 3800, Australia; ³Faculty of
9 Pharmacy and Pharmaceutical Sciences, Monash University, Melbourne 3052, Australia;
10 ⁴Monash Institute of Cognitive and Clinical Neurosciences, Department of Anatomy and
11 development biology, Faculty of Medicine, Nursing and Health Sciences, Monash University,
12 Melbourne 3800, Australia; ⁵Department of Computer and Information Science, University of
13 Konstanz, Konstanz 78457, Germany; ⁶Department of Pharmacology and Therapeutics,
14 University of Melbourne, Melbourne 3010, Australia.

15 **Email addresses:** YZ, yan.zhu@monash.edu; TC, tobias.czauderna@monash.edu; JZ,
16 jinxin.zhao@monash.edu; MK, matthias.klapperstueck@monash.edu; MHMM,
17 hafidz.maifiah@monash.edu; MLH, meiling.han@monash.edu; JLU, jing.lu2@monash.edu;
18 BS, bjoern.sommer@uni-konstanz.de; TV, tony.velkov@unimelb.edu.au; TL,
19 trevor.lithgow@monash.edu; JS, jiangning.song@monash.edu; FS, falk.schreiber@uni-
20 konstanz.de; JL, jian.li@monash.edu.

21 **Running title:** Metabolic modelling polymyxins responses

22 *Corresponding authors:

23 **Falk Schreiber**, Email: falk.schreiber@uni-konstanz.de

24 **Jian Li**, 19 Innovation Walk, Monash University, VIC 3800, Australia. Tel: +61 3 9903 9702,
25 Fax: +61 3 9902 9222, Email: jian.li@monash.edu.

1
2
3
4
5
6
7
8
9
10
11
12
13
14
15
16
17
18
19
20
21
22
23
24
25
26
27
28
29
30
31
32
33
34
35
36
37
38
39
40
41
42
43
44
45
46
47
48
49
50
51
52
53
54
55
56
57
58
59
60
61
62
63
64
65

26 Part of this work was presented at the 27th European Congress of Clinical Microbiology and
27 Infectious Diseases, 22-25 April 2017, Vienna, Austria.

28 **Abstract**

29 **Background:** *Pseudomonas aeruginosa* often causes multidrug-resistant infections in
30 immunocompromised patients and polymyxins are often used as the last-line therapy.
31 Alarming, resistance to polymyxins has been increasingly reported worldwide recently. To
32 rescue this last-resort class of antibiotics, it is necessary to systematically understand how *P.*
33 *aeruginosa* alters its metabolism in response to polymyxin treatment, thereby facilitating the
34 development of effective therapies. To this end, a genome-scale metabolic model (GSMM)
35 was employed to analyse bacterial metabolic changes at the systems level.

36 **Findings:** A high-quality GSMM *iPAO1* was constructed for *P. aeruginosa* PAO1 for
37 antimicrobial pharmacological research. Model *iPAO1* encompasses an additional periplasmic
38 compartment and contains 3,022 metabolites, 4,265 reactions and 1,458 genes in total. Growth
39 prediction on 190 carbon and 95 nitrogen sources achieved an accuracy of 89.1%,
40 outperforming all reported *P. aeruginosa* models. Notably, prediction of the essential genes for
41 growth achieved a high accuracy of 87.9%. Metabolic simulation showed that lipid A
42 modifications associated with polymyxin resistance exert a limited impact on bacterial growth
43 and metabolism, but remarkably change the physiochemical properties of the outer membrane.
44 Modelling with transcriptomics constraints revealed a broad range of metabolic responses to
45 polymyxin treatment, including reduced biomass synthesis, upregulated amino acids
46 catabolism, induced flux through the tricarboxylic acid cycle, and increased redox turnover.

47 **Conclusions:** Overall, *iPAO1* represents the most comprehensive GSMM constructed to date
48 for *Pseudomonas*. It provides a powerful systems pharmacology platform for the elucidation
49 of complex killing mechanisms of antibiotics.

1
2
3
4
50 **Keywords:** Genome-scale metabolic model; *Pseudomonas aeruginosa*; polymyxin; lipid A
51 modification; outer membrane

5
6
7
8
9
10
11
12
13
14
15
16
17
18
19
20
21
22
23
24
25
26
27
28
29
30
31
32
33
34
35
36
37
38
39
40
41
42
43
44
45
46
47
48
49
50
51
52
53
54
55
56
57
58
59
60
61
62
63
64
65
66
67
68
69
70
71
72
73

52 **Background**

53 *Pseudomonas aeruginosa* is a common multidrug-resistant (MDR) pathogen in immune-
54 compromised patients, cystic fibrosis patients and burns victims [1-6]. It possesses a large
55 genome (5.5-7.0 Mb), complex regulatory networks, remarkable metabolic versatility and an
56 extraordinary ability to survive extremely harsh conditions such as prolonged antibiotic
57 exposure [7, 8]. Polymyxins (i.e. polymyxin B and colistin) have been increasingly used as a
58 last-line therapy to treat infections caused by MDR *P. aeruginosa* [9]. Alarmingly, the
59 prevalence of polymyxin resistance in *P. aeruginosa* has increased worldwide over the past
60 few years [3, 10, 11].

61 The exact mode of action of polymyxins is not clear except the initial electrostatic and
62 hydrophobic interactions with lipid A, a component of the lipopolysaccharide (LPS) in the
63 bacterial outer membrane (OM). Subsequently, cell envelope is disorganised, cellular contents
64 leak, oxidative stress increases, and finally cell death occurs [2, 9, 12, 13]. After polymyxin
65 treatment, *P. aeruginosa* modifies its lipid A structure to attenuate the aforementioned
66 electrostatic interactions [14]. Our recent metabolomics data demonstrated that, apart from
67 lipid A modifications, numerous biochemical pathways are perturbed by polymyxin treatment,
68 indicating that the development of polymyxin resistance by *P. aeruginosa* involves a
69 complicated interplay of multiple cellular processes [15]. There are significant gaps in the
70 knowledge-base of the mechanisms of polymyxin activity and bacterial responses in *P.*
71 *aeruginosa*, thereby necessitating comprehensive investigations using systems pharmacology
72 approaches.

73 With the rapid development of genome-scale metabolic models (GSMMs) and the associated

1
2
3
4
5
6
7
8
9
10
11
12
13
14
15
16
17
18
19
20
21
22
23
24
25
26
27
28
29
30
31
32
33
34
35
36
37
38
39
40
41
42
43
44
45
46
47
48
49
50
74 flux balance analysis (FBA) methods, systematic investigations into the metabolic changes in
75 response to external nutrient alterations, genetic perturbations, and antibiotic treatments
76 become feasible [16-24]. Several studies employed transcriptomics data as constraints to
77 compute condition-specific metabolic flux changes in response to antibiotic treatments in MDR
78 bacteria, including *Acinetobacter baumannii* [25], *Mycobacterium tuberculosis* [26] and
79 *Yersinia pestis* [27]. For *P. aeruginosa*, four GSMMs have been constructed, iMO1056 [28],
80 Opt208964 [29], iMO1086 [30] and the latest iPae1146 [31]. iMO1056, Opt208964 and
81 iPae1146 employed SEED metabolite and reaction names; iMO1056 and Opt208964 are fully
82 accessible via Model SEED [29, 31, 32]; iMO1086 employed different identifiers (IR/RR plus
83 five digits for reactions and C/EC plus four digits for metabolites) [30]. The previous
84 applications of these models have included simulating the metabolic dynamics in cystic fibrosis
85 patients [33], elucidating the mechanisms of biofilm formation [34, 35], predicting potential
86 drug targets [36-38] and identifying the key genes controlling virulence factors [31]. As
87 important as they have been, these models have several overarching limitations. Those past
88 models (i) do not include a major cellular component, the periplasmic space; (ii) have poor
89 representation of glycerophospholipid (GPL) biosynthesis; and (iii) lack lipid A modification
90 reactions. Considering the pathogenesis of *P. aeruginosa*, these major limitations significantly
91 compromise the modelling functions. In particular, the power of the four reported GSMMs
92 to predict metabolic responses to antibiotic treatment is very limited, as periplasmic GPL and
93 LPS biogenesis play critical roles in responses to anti-pseudomonal antibiotics such as
94 polymyxins [15, 39-42].

51
52
53
54
55
56
57
58
59
60
61
62
63
64
65
95 Here we describe *iPAO1*, a newly developed GSMM for *P. aeruginosa* PAO1 based upon
96 Opt208964 [29] and iMO1056 [28] but with intensive manual curation using several major
97 databases and the literature. Most notably, *iPAO1* is the first GSMM for *P. aeruginosa* where
98 the periplasmic space compartment is incorporated to comprehensively represent cross-

99 membrane transport, GPL metabolism and LPS biosynthesis. To the best of our knowledge
100 *i*PAO1 represents the most comprehensive metabolic reconstruction for *Pseudomonas* thus far.
101 Modelling with *i*PAO1 revealed that the lipid A modifications might exert limited impact on
102 cell growth and metabolism but change the physiochemical properties of bacterial OM.
103 Constrained by gene expression levels, the model was employed to elucidate the metabolic
104 responses to polymyxin B treatment. Together, *i*PAO1 provides a powerful systems platform
105 for antimicrobial pharmacological research to combat the rapidly increasing resistance.

107 **Data Description**

108 The genome sequence and annotation of *P. aeruginosa* PAO1 were obtained from GenBank
109 (Accession NC_002516.2). Models iMO1056 and Opt208964 were retrieved from Model
110 SEED [32]. The gas chromatography–mass spectrometry (GC-MS) metabolomics data were
111 collected from the literature [43]. Metabolites, reactions and pathways were obtained from
112 databases KEGG (Kyoto Encyclopaedia of Genes and Genomes) [44], MetaCyc [45], TCBD
113 (Transporter Classification Database) [46], TransporterDB [47] and *Pseudomonas* Genome DB
114 [48]. Growth phenotypes on 190 carbon sources and 95 nitrogen sources were determined using
115 BIOLOG Phenotypic Microarrays. Non-essential gene lists were collected from two previously
116 reported transposon mutant libraries for PAO1 [49, 50]. Lipid A of wild-type *P. aeruginosa*
117 PAK and its polymyxin-resistant mutant PAK $\textit{pmrB6}$ was extracted using mild acid hydrolysis
118 method and the structural analysis of lipid A was conducted using mass spectrometry [42].
119 RNA was extracted and employed to construct cDNA libraries for RNA-Seq on Illumina
120 MiSeq platform [51]. The raw reads were quality trimmed and aligned to PAO1 reference
121 genome using SubRead [52]. Counts were normalised and the differential gene expression was
122 determined using voom/limma packages with Degust [53]. Whole-cell lipids and intracellular
123 metabolites were extracted using the single-phase Bligh-Dyer method as previously described

124 and analysed by liquid chromatography-mass spectrometry (LC-MS) [14, 42]. Raw
125 metabolomics data were processed with IDEOM software followed by bioinformatics analysis
126 [54].

127

128 **Analyses**

129 **Development of a superior GSMM for *P. aeruginosa* PAO1**

130 Initially, a draft model (*i*PAO1_draft1) containing 1,991 reactions, 1,579 metabolites and 1,021
131 genes was created based upon iMO1056 [28] and Opt208964 [29] (**Additional files 2-4**). To
132 obtain a high-quality GSMM, extensive manual curation was conducted. Firstly, *i*PAO1_draft1
133 was complemented using databases and the literature. Specifically, the following additional
134 information was incorporated into the draft model, 285 metabolites and 36 reactions from
135 KEGG [44], 225 metabolites and 50 reactions from MetaCyc [45], and 7 metabolites and 20
136 reactions obtained by previous GC-MS-based quantification [43] (**Additional files 5 and 6**).

137 Secondly, a periplasmic compartment was built to incorporate 698 periplasmic metabolites,
138 509 transport reactions across the inner membrane (IM), 441 transport reactions across the
139 outer membrane (OM), and 403 periplasmic reactions. The resulting intermediate model was
140 designated as *i*PAO1_draft2.

141 Thirdly, the major pathway gaps were filled. GapFind [55] identified 109 dead-end metabolites
142 (**Additional file 7**). The growth phenotypes on 190 carbon and 95 nitrogen nutrients were
143 predicted using *i*PAO1_draft2, and compared with our experimental BIOLOG Phenotypic
144 Microarray (PM) results (**Additional file 8**). As a result, 162 false negative predictions (i.e. the
145 prediction indicated non-growth whereas the BIOLOG experiment demonstrated valid growth
146 on a specific nutrient) were determined, indicating the lack of associated transport or catabolic
147 reactions for these nutrients. To link the dead-end metabolites back to the metabolic network

148 and eliminate inconsistencies with the BIOLOG PM results, several modifications were made
1
2 including (i) adjustment of the reversibility settings of 180 reactions and changing the
3
4 directions of 87 reactions (**Additional file 9**); (ii) removal of 14 metabolites and 96 reactions
5
6 (**Additional files 10 and 11**), which were either duplicated (e.g. β -D-glucose was duplicated
7
8 with D-glucose) or representing general metabolite classes (e.g. protein, mRNA, DNA); and
9
10
11
12 (iii) addition of 98 boundary reactions, 677 transport reactions, and 252 metabolic reactions
13
14 (**Additional file 12**). Resolving the false negative predictions of the BIOLOG growth
15
16 phenotypes substantially improved the model. For example, predictions using *iPAO1_draft2*
17
18 showed that PAO1 was unable to grow with formic acid as a sole carbon source due to the lack
19
20 of the corresponding transport reaction. Interrogating the Pseudomonas Genome Database [48]
21
22 and Pfam [56] identified PA2777, a hypothetical protein in NCBI and UniProt which may
23
24 encode formic/nitrite transporter (Pfam01226, $P=7e-34$). Subsequent addition of the transport
25
26 reaction (rxn08526) enabled *in silico* growth of PAO1 on formic acid. Another example is that
27
28 initially *iPAO1_draft2* failed to predict utilisation of 1,2-propanediol for growth owing to the
29
30 exiting gap in dehydrogenation of 1,2-propanediol to lactaldehyde. Using BLASTp with the
31
32 query sequence of lactaldehyde reductase (*fucO*, *b2799*) from *Escherichia coli* K12 MG1655
33
34 identified a candidate homologous gene PA1991 (Identity=35%, Eval=2e-75, BLASTp).
35
36 PA1991 encodes an iron-containing alcohol dehydrogenase and has over 300 orthologues in
37
38 Gram-negative bacteria which encode lactaldehyde oxidoreductases or 1,2-propanediol
39
40 dehydrogenases according to OrthoDB [57]. Inactivation of PA1991 resulted in 8-fold
41
42 prolonged lag phase when *P. aeruginosa* grew on 1,2-propanediol [58]. Therefore, reaction
43
44 rxn01615 oxidising 1,2-propanediol to lactaldehyde was added into *iPAO1_draft2*. A very
45
46 large number of such labour intensive manual curations were conducted to improve the model.
47
48 This enabled *in silico* growth on a number of nutrients from BIOLOG PM, including 4-
49
50 hydroxyphenylacetate, tyramine, quinic acid, itaconic acid, citramalic acid, L-pyroglutamic
51
52
53
54
55
56
57
58
59
60
61
62
63
64
65

173 acid, carnidine, glycinebetaine, L-methylsuccinate, and D-amino acids (**Additional file 8**).

174 Fourthly, the biogenesis of bacterial envelope was delineated. Cross-linking between amino
175 acids residues among peptidoglycan chains results in a rigid network structure in *P. aeruginosa*
176 [59]. In total, 17 reactions representing peptidoglycan cross-linking and hydrolysis were
177 incorporated by searching for homologues of glycosyltransferases, transpeptidases,
178 carboxypeptidases and endopeptidases in PAO1 [60]. Overall, a detailed peptidoglycan
179 biosynthesis pathway was constructed with 60 reactions. GPL compositions in the bacterial
180 membranes can change in response to antibiotic treatment [39, 61]. Previous studies [62] and
181 our own lipidomics results [14] showed a great diversity in GPL species in *P. aeruginosa*.
182 Overall, 386 unique metabolites (i.e. 66.2% of the 583 metabolites in the GPL metabolism
183 pathway) and 367 reactions (66.7% of the 550 reactions in the GPL metabolism pathway) were
184 incorporated into *iPAO1_draft2* (**Additional files 1, 13 and 14, Fig 1**). LPS consists of lipid
185 A, core oligosaccharide, and *O*-antigen polysaccharide [40], and plays key roles in the host-
186 pathogen interaction and the resistance to antibiotics such as polymyxins [13, 63]. A detailed
187 synthesis and interconversion network was generated with 432 types of LPS and 1,169
188 reactions (**Fig 2, Additional file 1**). Notably, our GSMM is the most comprehensive to date in
189 lipid A biosynthesis and modifications.

190 The resulting final *iPAO1* model consisted of 3,022 metabolites, 4,365 reactions and 1,458
191 genes (25.8% of the PAO1 genome, **Additional files 15-17**), representing, respectively, (i)
192 252%, 340% and 40% increase of the components in *iMO1056*; and (ii) 125%, 171% and 43%
193 increase of the components in *Opt208964* (**Table 1**). The significant expansion in *iPAO1*
194 includes cross-membrane transport, GPL/LPS biosynthesis, peptidoglycan biosynthesis, and
195 fatty acid degradation (**Additional files 15-17**). The reactions from *iPAO1* were categorised
196 into 109 pathways mainly based on classifications in MetaCyc and KEGG. In *iPAO1*,
197 27.9%/43.7%/51.6% metabolites, 20.3%/33.5%/59.5% reactions and 65.3%/17.6%/28.5%

198 genes are originated from iMO1056, Opt208964, and our manual curation, respectively (**Fig**
199 **3A**).

200 Components in *iPAO1* were aligned with databases including KEGG [44], MetaCyc [45],
201 PubChem [64], ChemSpider [65], ChEBI [66], Model SEED [32], and BiGG [67] (**Additional**
202 **files 15 and 16**). Consequently, 1,404 (46.5%), 1,590 (52.6%) and 2,142 (70.9%) metabolites
203 have corresponding identifiers in MetaCyc, KEGG and Model SEED, respectively; 1,556
204 (35.6%), 1,596 (36.6%) and 1,964 (45.0%) reactions were computationally mapped to the
205 reactions from MetaCyc, KEGG and Model SEED, accordingly (**Fig 3B**). A significant portion
206 of mismatches were caused by the incorporation of specific types of metabolites in the GPL
207 metabolism and LPS biosynthesis pathway, which in databases are usually lumped as general
208 compound classes. The properties of metabolites, including mass, charge and formula were
209 included in *iPAO1*. The standard Gibbs free energy change of formation ($\Delta_f G^\circ$), and reaction
210 ($\Delta_r G^\circ$) were obtained from MetaCyc and Model SEED for 1,877 metabolites (62.1%) and 1,355
211 reactions (31.0%) (**Additional files 15 and 16**).

212 A breakdown of genes involved in *iPAO1* (**Additional file 17**) using the clusters of orthologous
213 groups (COGs) showed remarkable improvement compared to previous reconstructions (**Fig**
214 **3C**). The largest increase in the coverage compared to iMO1056 is lipid transport and
215 metabolism (24.1%), followed by inorganic ion transport and metabolism (19.3%); whereas
216 compared to Opt208964, the largest increase in the coverage is nucleotide transport and
217 metabolism (57.9%), followed by amino acid transport and metabolism (52.0%). Overall, the
218 transport and metabolism of nucleotides and amino acids showed the highest percent coverage
219 of COG functional categories in *iPAO1* (72.9% and 65.6%, respectively). Notably, the
220 reactions in categories not apparently related to metabolism were dramatically reduced in
221 *iPAO1* compared to Opt208964, including translation, ribosomal structure and biogenesis,
222 posttranslational modification, protein turnover, chaperones and signal transduction

223 mechanisms, or undetermined categories including function unknown class.

224 In *iPAO1*, GPL metabolism, LPS biosynthesis and transport across OM were ranked the three

225 largest pathways and also contained the highest proportion of curated reactions (**Fig 3D**).

226 Additionally, these three pathways have high reaction-to-gene ratios (13.1-24.2, **Fig 3E**),

227 indicating that enzymes in these pathways are capable of acting on a broad range of substrates.

228 As kinetic parameters are usually not involved in a GSMM, constraint-based analyses (e.g.

229 FBA) of a GSMM do not directly account for enzyme levels, intracellular metabolic

230 concentrations or substrate-level regulation. Accordingly, the affinity difference of various

231 substrates was not considered in our *iPAO1* modelling effort.

232 We employed the biomass formation equation from iMO1056 to construct *iPAO1* with

233 modifications on LPS and ion species (**Additional file 18**). In addition, to take into account the

234 extra energy consumption caused by charging tRNAs, the original amino acids in the biomass

235 formation reaction were replaced by aminoacyl-tRNA, followed by addition of specific

236 charging reactions to the model. Taken together, *iPAO1* represents the most comprehensive

237 metabolic reconstruction thus far for *P. aeruginosa* PAO1.

238 **Growth capability on various nutrients**

239 Investigation of nutrient utilisation using BIOLOG PM showed PAO1 could utilise a broad

240 range of nutrient sources, indicated by the observed growth on 68 of 190 (35.8%) carbon and

241 76 of 95 (80.0%) nitrogen substrates (**Fig 4**). Growth simulation with *iPAO1* achieved an

242 overall accuracy of 89.1% (254 of 285), which substantially outperformed previous models

243 (81.5% for Opt208964 [29], 77.9% for iMO1056 and iMO1086 [30] and 80% for iPae1146

244 [31]. Twenty-one false-positive and 10 false-negative (**Fig 4, Additional file 8**) disagreements

245 were observed, possibly due to the complexity of regulatory mechanisms and missing

246 annotation of nutrient transport and/or catabolism pathways in PAO1.

247 Prediction and validation of gene essentiality

1
2
3 248 *In silico* single-gene deletion with *iPAO1* showed 143 essential genes ($\mu_{\text{mut}} < 0.01 \mu_{\text{wt}}$), 40 semi-
4
5 249 essential genes ($0.01 \mu_{\text{wt}} < \mu_{\text{mut}} < 0.99 \mu_{\text{wt}}$), and 1,275 non-essential genes ($0.99 \mu_{\text{wt}} < \mu_{\text{mut}} < \mu_{\text{wt}}$)
6
7
8 250 when growing in Luria-Bertani (LB) media (**Additional file 19**). Among the essential
9
10 251 metabolic genes, the largest COG proportion (46 of 143, 32.1%) is cell envelope biogenesis,
11
12 252 indicating that there are relatively less alternative reactions in this pathway. For non-essential
13
14
15 253 genes, amino acid transport and metabolism (352 of 1,315, i.e. 26.7%) represents the largest
16
17 254 group, suggesting the existence of large metabolic redundancy.

18
19
20 255 The predicted gene essentiality was further verified by two independent genome-scale
21
22 256 transposon mutant libraries [49, 50, 68]. The overall prediction accuracy achieved 87.9%,
23
24
25 257 which is higher than iMO1056 (85.0%) [28] and iMO1086 (84.2%) [30], but slightly lower
26
27
28 258 than Opt208964 (92.9%) [29] and iPae1146 (91.46%) [31]. The higher accuracy in Opt208964
29
30 259 is partially due to errors in the annotation of essential genes. For instance, 351 genes in
31
32 260 Opt208964 were grouped as experimentally validated essential; however, 145 out of the 351
33
34
35 261 genes are non-essential as their corresponding mutants were found in the transposon mutant
36
37 262 library [50]. In iPae1146, removal of 16 isozymes increased the prediction accuracy of essential
38
39
40 263 genes; for example, 3-ketoacyl-ACP reductase (EC 1.1.1.100) reactions in iPae1146 were
41
42 264 associated with PA2967 only [31], whereas in *iPAO1*, these reactions were associated with
43
44
45 265 another eight highly conserved isozymes (PA0182, PA1470, PA1827, PA3387, PA4089,
46
47 266 PA4389, PA4786, PA5524). Furthermore, condition-specific essential genes were predicted in
48
49
50 267 *iPAO1* by imposing transcriptomics constraints. Modification of lipid A with 4-amino-4-
51
52 268 deoxy-L-arabinose (L-Ara4N) leads to polymyxin resistance in *P. aeruginosa* and deficiency
53
54
55 269 in *arn* genes reverses the susceptibility [69]. Seven additional essential genes (*arnABCDEFT*,
56
57 270 PA3552-3558, encoding L-Ara4N biosynthesis) were predicted by *iPAO1* under polymyxin
58
59 271 treatment.
60
61
62
63
64
65

272 Impact of lipid A modifications on bacterial growth and metabolism

1
2
3 273 *P. aeruginosa* modifies lipid A components in the OM in response to polymyxin treatment [70].
4

5 274 The LPS stoichiometric coefficients in the biomass formula of *i*PAO1 were configured based
6

7
8 275 on our lipidomics data (**Table 2**, [14]), and the metabolic impact of lipid A modifications was
9

10 276 predicted by randomly sampling the metabolic solution space with 10,000 points (*cf.* Methods).
11

12 277 Overall, 273 fluxes were significantly affected (Z-Score, false discovery rate (FDR)
13

14
15 278 <0.01 ; >0.1 mmol·gDW⁻¹·h⁻¹ under at least one condition, **Additional file 20**). The specific
16

17
18 279 growth rate remained unchanged. A 0.026 mmol·gDW⁻¹·h⁻¹ flux from glucose via glucose 6-
19

20 280 phosphate, uridine diphosphate glucose, and consequently L-Ara4N biosynthesis was
21

22 281 identified due to lipid A modifications. The overall fluxes through lipid A deacylation reactions
23

24
25 282 were increased (from 0.007 mmol·gDW⁻¹·h⁻¹ to 0.011 mmol·gDW⁻¹·h⁻¹); the generated (*R*)-3-
26

27
28 283 hydroxydecanoate was fuelled into β -oxidation to produce octanoyl-CoA, which was
29

30 284 subsequently salvaged for fatty acid biosynthesis.
31

32
33 285 To further investigate the impact of lipid A modifications on bacterial growth, 1,000 sets of the
34

35 286 compositions of 288 heterogeneous LPS molecules were randomly generated with the total
36

37
38 287 proportion of LPS unchanged in the biomass formation formula (**Additional file 21**). The
39

40 288 metabolic fluxes were calculated for each of the 1,000 sets of LPS compositions by randomly
41

42
43 289 sampling the solution space with 10,000 points. Across the 1,000 sets of metabolic fluxes
44

45 290 (**Additional file 23**), the specific growth rate varied between 0.8812 and 0.8897 mmol·gDW⁻¹·h⁻¹.
46

47
48 291 Correlative analysis of the apparent overall physiochemical properties of lipid A
49

50 292 (**Additional file 22**) with the predicted growth phenotypes showed three interesting findings.
51

52
53 293 Firstly, addition of L-Ara4N reduced the negative charge of lipid A ($\rho=1.00$), decreased the
54

55 294 hydrophobicity of the OM (represented by logP, $\rho=-0.59$), but required assimilation of more
56

57
58 295 ammonia (represented by ammonia turnover, $\rho=0.57$). Secondly, hydroxylation on acyl chains
59
60
61
62
63
64
65

296 of lipid A exerted minor effects over either bacterial growth or physiochemical properties.
297 Thirdly, addition of acyl chains resulted in large lipid A molecules (represented by the atomic
298 counts, $\rho=0.88$), enhanced molecular polarity of lipid A ($\rho=0.87$), increased OM
299 hydrophobicity ($\rho=0.75$), and notably, retarded growth ($\rho=-0.95$), reduced redox and energy
300 turnover ($\rho=-0.98$ for both), and increased requirement of ammonia ($\rho=0.59$) (**Fig 5**). It is
301 evident that none of the three aforementioned modifications produced a dramatic impact on
302 bacterial growth or metabolism (**Additional file 23**).

303 **Elucidating the mechanisms of metabolic responses to polymyxin treatment**

304 RNA-Seq data were utilised as model constraints (**Additional file 24**) with an E-Flux method
305 [71] to calculate the metabolic fluxes in the absence and presence of polymyxin B (*cf.* Methods).
306 The exchange fluxes were constrained based on the maximum uptake rates of the media
307 ingredients (*cf.* Methods and **Additional file 1**). Comparison of the flux distributions revealed
308 that 1,392 reactions were differentially regulated ($FDR < 0.01$, **Additional file 25**). A range of
309 metabolic pathways were significantly disturbed, including central metabolism, amino acid
310 metabolism, purine biosynthesis, fatty acid biosynthesis and metabolism, LPS and GPL
311 biosynthesis and transport reactions. Polymyxin B treatment reduced the growth rate (18.2%),
312 increased oxygen uptake (6.9%) and CO₂ emission (6.0%); however, the respiration quotient
313 remained roughly unchanged (**Table 3**).

314 As the major carbon sources, the amino acids and oligopeptides from cation-adjusted Mueller-
315 Hinton broth (CAMHB) were utilised to generate intermediate metabolites, redox and energy
316 equivalents for biomass formation. In response to polymyxin treatment, the gluconeogenesis
317 pathway was significantly induced from pyruvate to 3-phosphoglycerate, but suppressed from
318 3-phosphoglycerate towards glucose 6-phosphate. The extra flux from 3-phosphoglycerate was
319 shunt to serine and glycine biosynthesis (**Fig 6**) via 3-phospho-D-glycerate:NAD⁺

320 oxidoreductase (rxn01101), 3-phosphoserine:2-oxoglutarate aminotransferase (rxn02914), *O*-
321 phospho-L-serine phosphohydrolase (rxn00420), and 5,10-methylenetetrahydrofolate:glycine
322 hydroxymethyltransferase (rxn00692), through which more NADH equivalent was generated
323 compared to the control (i.e. growth in CAMHB without polymyxin treatment). The resulting
324 one-carbon unit in 5,10-methylenetetrahydrofolate was oxidised to formic acid via 10-
325 formyltetrahydrofolate amidohydrolase (rxn00691); the generated glycine was fuelled into
326 TCA cycle via glycine:oxygen oxidoreductase (rxn00269) and acetyl-CoA:glyoxylate C-
327 acetyltransferase (rxn00330). In addition, the metabolic flux via TCA cycle was upregulated
328 from citrate to fumarate, with increased NADH production. Within oxidative phosphorylation,
329 the mean fluxes through NADH dehydrogenase (Complex I, rxn10122), cytochrome bc1
330 complex (Complex III, rxn13820), and cytochrome c oxidase (Complex IV, rxn13688)
331 decreased by 6.6%, 7.2% and 7.8%, respectively. The flux via F₀F₁-ATPase (Complex V,
332 rxn10042) was downregulated by 11.1%. The overall fluxes via biosynthesis of
333 macromolecules including LPS, GPL and peptidoglycan decreased due to the significantly
334 reduced biomass formation. The biosynthesis of spermidine increased by 38.3% in response to
335 polymyxin treatment which was also indicated by upregulated expression of *speD* (PA4773;
336 encoding the *S*-adenosyl-L-methionine decarboxylase, log₂FC=3.62, FDR<0.01) and *speE*
337 (PA4774; encoding spermidine synthase, log₂FC = 3.54, FDR<0.01).

338 Calculating the flux-sum of critical cofactors revealed 13.1% increase of redox turnover and
339 8.2% decline of energy turnover after 1 mg·L⁻¹ polymyxin B treatment for 1 h. Breaking down
340 the cofactors showed the turnover of major redox equivalents NADH, NADPH, ubiquinol-8
341 and FADH₂ substantially increased by 12.6%, 13.9%, 3.9% and 35.9%, respectively; whereas
342 the turnover of ATP, the major contributor to energy significantly decreased by 8.52% after 1
343 mg·L⁻¹ polymyxin treatment for 1 h (**Fig 6, Additional file 26**). Overall, metabolic flux analysis
344 using *i*PAO1 integrated with our transcriptomics data revealed a significant global impact on

1
2
3 345 bacterial metabolism due to polymyxin B treatment.
4

5
6 346

7
8
9 347 **Discussion**

10
11 348 The emergence of Gram-negative ‘superbugs’ that are resistant to the last-resort polymyxins
12
13 349 highlights the urgent need for novel approaches such as GSMMs to understand the mechanisms
14
15 350 of antibacterial activity and resistance. The main utility of GSMMs is their ability to bridge
16
17 351 critical gaps between genomics and metabolic phenotypes through the prediction of metabolic
18
19 352 responses to antimicrobial treatments at the network level. Here, we report the development,
20
21 353 optimisation, validation and application of a high-quality GSMM designated *iPAO1* for a type
22
23 354 strain *P. aeruginosa* PAO1; and importantly, *iPAO1* was employed to understand the
24
25 355 complicated effect of polymyxin treatment on bacterial metabolism. Simulation with *iPAO1*
26
27 356 showed that lipid A modifications in response to polymyxin treatment only exert minor effects
28
29 357 on bacterial growth and metabolism. Albeit, further calculations that integrate transcriptomics
30
31 358 data as model constraints revealed that polymyxin treatment may reduce growth and affect a
32
33 359 broad range of pathways.
34
35
36

37
38 360 *iPAO1* represents the most comprehensive metabolic model for *P. aeruginosa* to date and
39
40 361 incorporates 1,458 genes, accounting for ~25.8% of the PAO1 genome. Among the four
41
42 362 GSMMs developed for *P. aeruginosa* PAO1, iMO1086 and iPae1146 were constructed on the
43
44 363 basis of iMO1056 with moderate increase of metabolites, reactions and genes [28, 30, 31];
45
46 364 Opt208964 is also in a medium size, which limits modelling capacity [29]. In contrast, *iPAO1*
47
48 365 is significantly expanded in model scale, by doubling or even tripling the numbers of
49
50 366 metabolites and reactions (**Fig 3A**). *iPAO1* achieved an unprecedented prediction accuracy of
51
52 367 89.1% for growth on various nutrients, outperforming all of the previously reported GSMMs
53
54 368 for *P. aeruginosa* [28-31]. The *iPAO1* model was also employed to predict gene essentiality
55
56
57
58
59
60
61
62
63
64
65

369 with a high accuracy of 87.9%. Given the extensive curation and significant expansion, *iPAO1*
370 will serve as the primary reference for future development of metabolic models, particularly
371 for other *P. aeruginosa* strains.

372 Unlike *iPAO1*, none of the previous *P. aeruginosa* GSMMs incorporated the periplasm. As
373 polymyxins initially target LPS in the OM and can cause substantial changes in the cell
374 envelope, the periplasmic space is a major component in *iPAO1*. The periplasmic space of *E.*
375 *coli* is estimated to constitute up to 16% of total cell volume [72]. It contains a thin cell wall
376 composed of peptidoglycan and a variety of ions and proteins, which are involved in transport,
377 folding, cell envelope biogenesis, electron transport and xenobiotic metabolism [73]. *iPAO1* is
378 the first *P. aeruginosa* GSMM to incorporate the periplasmic compartment, enabling accurate
379 representation of metabolic machinery, especially for those reactions that occur exclusively in
380 this important cellular space and transport of substrates across the IM and OM. Furthermore,
381 *iPAO1* provides detailed representations of GPL and LPS biosynthesis which allows the
382 precise mapping of GPL and LPS responses from experimental metabolomics and lipidomics
383 data (**Figs 1 and 2**).

384 In response to polymyxin treatment, Gram-negative bacteria modify their lipid A with cationic
385 moieties (i.e. phosphoethanolamine and L-Ara4N) that act to repel the like-charge of the
386 polymyxin molecule [40]. Based on our simulations (**Additional file 20**), we purport that such
387 lipid A modifications exerted a limited impact on cellular metabolism and growth. Most of the
388 flux changes were insignificant; the remaining significant flux changes mainly resulted from
389 futile cycles containing sets of reactions using redox equivalents, whereas the net carbon flow
390 remained unchanged. Simulation using randomised lipid A compositions further consolidated
391 our hypothesis that lipid A modifications cause only moderate variations of bacterial growth
392 and metabolism (**Fig 5, Additional file 23**). Notwithstanding, our simulation results revealed
393 that lipid A modifications result in substantial physiochemical changes in the OM of *P.*

1
2
3
4
5
6
7
8
9
10
11
12
13
14
15
16
17
18
19
20
21
22
23
24
25
26
27
28
29
30
31
32
33
34
35
36
37
38
39
40
41
42
43
44
45
46
47
48
49
50
51
52
53
54
55
56
57
58
59
60
61
62
63
64
65

394 *aeruginosa*, including (i) neutralising the surface negative charge by addition of positively
395 changed L-Ara4N; and (ii) altering the polarity and hydrophobicity by acylation and
396 deacylation. The general mode of action of polymyxin involves the initial electrostatic
397 interaction between the cationic side chains of the polymyxin molecule with the anionic lipid
398 A head groups [63]. These events are subsequently followed by hydrophobic interactions
399 between the *N*-terminal fatty acyl chain and position 6/7 hydrophobic side chains of the
400 polymyxin with the hydrophobic fatty acyls of lipid A [63]. Therefore, in concept both the
401 addition of L-Ara4N and deacylation of lipid A should contribute to polymyxin resistance.
402 Indeed, our recent transcriptomic and neutron reflectometry studies discovered that deletion of
403 the corresponding gene *pagL* (PA4661) resulted in an increased susceptibility to polymyxins,
404 in a polymyxin-resistant mutant PAK*pmrB6* derived from *P. aeruginosa* PAK [14, 74],
405 demonstrating that the lipid A deacylation also plays a key role in the response of *P. aeruginosa*
406 to polymyxin treatment.

407 Our recent transcriptomics and metabolomics studies discovered that polymyxin treatment
408 leads to remarkable growth reduction and metabolic perturbations in Gram-negative bacteria
409 [41, 42, 75-77]. The integration of transcriptomics results into GSMMs allow for more accurate
410 predictions of metabolic responses to either environmental (i.e. antibiotic treatment) or genetic
411 perturbations (i.e. mutations) [78]. In the present study, we employed the E-Flux method to
412 integrate transcriptomics data as flux constraints [26]. E-Flux can map continuous gene
413 expression levels to the metabolic network and uses the transcript abundance to determine the
414 degree to which a reaction is active or inactive [26]. Therefore, E-Flux provides a more
415 physiologically relevant description of the continuous nature of the reaction activity and avoids
416 to use any artificial thresholds to binarise gene expression data [79]. In the present study,
417 metabolic fluxes with and without antibiotic treatment were not be calculated with
418 Minimization Of Metabolic Adjustment (MOMA), as MOMA was developed to predict the

1 419 metabolic flux redistributions in gene knockout mutants [80]. MOMA hypothesises that
2 420 metabolism of the mutant tends to approximate the wild-type [80], which is distinct from the
3
4 421 antibiotic treatment scenario. For instance, our metabolomics data have demonstrated that the
5
6
7 422 antibiotic treatment caused dramatic metabolic changes in bacteria [41].
8
9

10 423 Comparison of the calculated flux distributions revealed that a broad range of metabolic
11
12 424 perturbations occur in response to polymyxin treatment (**Fig 6**), ranging from central carbon
13
14
15 425 metabolism to oxidative phosphorylation and amino acid metabolism. Reduced growth,
16
17 426 increased redox turnover and decreased energy turnover due to polymyxin treatment were
18
19
20 427 evident (**Fig 6**), indicating that bacterial cells regulated their metabolism to produce more redox
21
22 428 power to cope with the oxidative stress. This is consistent with previous findings that showed
23
24
25 429 bactericidal antibiotics induced lethal oxidative damages via generating highly deleterious free
26
27 430 radicals with subsequent culmination of cellular death [81]. In addition, our simulations
28
29
30 431 revealed that polymyxin treatment induced an uptake of L-alanine, which was catabolised to
31
32 432 generate more NADH (**Fig 7**). This indicates that rich media (e.g. CAMHB) may provide
33
34 433 abundant amino acids and peptides that can be utilised by bacterial cells to generate sufficient
35
36
37 434 redox equivalents to cope with the oxidative damage caused by polymyxin treatment.
38
39 435 Furthermore, our simulation results also showed an upregulated metabolic flux towards L-
40
41
42 436 spermidine biosynthesis upon polymyxin B treatment (rxn00127 and rxn01406, **Additional**
43
44 437 **file 25**). Previous studies showed that polyamines (e.g. spermidine) could protect *P. aeruginosa*
45
46 438 from antimicrobial peptide killing [82]. It is assumed that the cationic spermidine could interact
47
48
49 439 with the anionic LPS, mask the negative cell surface, and reduce the electrostatic interactions
50
51
52 440 between polymyxin B and bacterial OM. Therefore, the enhanced biosynthesis of spermidine
53
54 441 might increase its abundance at the cell surface and contribute to polymyxin resistance.

55
56
57 442 The constructed *iPAO1* provides a detailed presentation of LPS biogenesis (**Fig 2**), in particular
58
59 443 lipid A modifications. Further integration with specific regulatory modules will enable
60
61
62
63
64
65

1
2
3
4
5
6
7
8
9
10
11
12
13
14
15
16
17
18
19
20
21
22
23
24
25
26
27
28
29
30
31
32
33
34
35
36
37
38
39
40
41
42
43
44
45
46
47
48
49
50
51
52
53
54
55
56
57
58
59
60
61
62
63
64
65

444 dynamic simulation of metabolic responses to polymyxin treatment. Previous studies revealed
445 that various two-component regulatory systems (2CSs), including PhoPQ, PmrAB, ParRS,
446 CprRS and ColRS, play key roles in regulating polymyxin resistance [69, 83-86]. Among them,
447 the PmrAB and PhoPQ systems are able to sense the depletion of external cations (e.g. Mg²⁺
448 and Ca²⁺) and upregulate the expression of the *arnBCADTEF-ugd* operon which is responsible
449 for the modification of lipid A with L-Ara4N [87]. Moreover, the fatty acylation of lipid A by
450 PagP is under the control of PhoPQ [88, 89]. ParRS and CprRS are independent 2CSs that
451 mediate the upregulation of *pmrAB*, *arnBCADTEF-ugd* operon, *pagL* and adaptive resistance
452 in response to polymyxin treatment [83, 90]. In overview, lipid A modifications due to
453 polymyxin treatment are strictly controlled by very complex regulatory networks involving
454 signal sensors, transcriptional regulators, and metabolic enzymes. Therefore, future studies are
455 warranted to integrate these regulatory modules into the GSMM to enable simulating bacterial
456 response dynamics to polymyxin treatment and analysing adaptive resistance mechanisms in
457 *P. aeruginosa*.

458 Overall, we have constructed, optimised and validated a high-quality genome-scale metabolic
459 model *iPAO1* for *P. aeruginosa* PAO1. This comprehensive model incorporates metabolic
460 pathways, particularly the biogenesis of membrane components, and enables delineating the
461 complex metabolic responses to antibiotics. *iPAO1* provides a valuable systems tool for
462 quantitative simulation of bacterial metabolic responses to antibiotics, elucidation of the
463 molecular mechanisms of antimicrobial killing and resistance, and facilitation of designing
464 rational antimicrobial combination therapy. To the best of our knowledge, this study is the first
465 to integrate antimicrobial pharmacology, computational biology, metabolic network and
466 systems pharmacology to analyse large-scale datasets, in order to better understand the
467 dynamic and complex nature of polymyxin killing and resistance. Combined with antibiotic
468 pharmacokinetics and pharmacodynamics, *iPAO1* offers an *in silico* platform for precision

1
2
3 469 polymyxin chemotherapy.

4
5
6 470

7 8 9 471 **Potential implications**

10
11 472 The generated collection of transcriptomics metabolomics, lipidomics and lipid A profiling
12
13 473 data provides comprehensive datasets of *P. aeruginosa* for future integrative analysis of
14 474 polymyxin systems pharmacology. As the largest curated GSMM thus far for *Pseudomonas*,
15
16 475 *i*PAO1 represents all aspects of the cellular metabolism and may serve as the platform for
17
18 476 integrative analysis of multi-omics data. Simulation with transcriptomics constraints in this
19
20
21 477 study revealed metabolic flux changes in amino acid catabolism, tricarboxylic acid cycle, and
22
23 478 redox turnover caused by polymyxin treatment. Correlative analysis of metabolomics and
24
25
26 479 transcriptomics with the constraint-based modelling is necessary for delineating the regulatory
27
28 480 effects on metabolism. The methodology of using GSMMs to analyse multi-level omics data
29
30
31 481 is applicable to other areas beyond antimicrobial pharmacology. Further integration with
32
33 482 antimicrobial pharmacokinetics and pharmacodynamics will not only provide better
34
35 483 pharmacological understanding, but also empower the model to quantitatively predict the
36
37
38 484 bacterial responses to antimicrobial therapy in the context of complex interplay of signalling,
39
40 485 transcriptional regulation and metabolism. In summary, our GSMM approach provides a
41
42
43 486 powerful systems tool to elucidate the complex mode of action of antibiotics and will paradigm
44
45 487 shift antimicrobial pharmacology.

46
47
48 488

49 50 51 489 **Methods**

52 53 54 490 **Strain, media and BIOLOG experiments**

55
56
57 491 *P. aeruginosa* PAO1 was cultured in Luria-Bertani (LB) media and subcultured on nutrient
58
59 492 agar. Cells were swapped into sterile capped tube containing 16 mL IF-0 solution (Cell
60
61
62
63
64
65

1
2
3
4
5
6
7
8
9
10
11
12
13
14
15
16
17
18
19
20
21
22
23
24
25
26
27
28
29
30
31
32
33
34
35
36
37
38
39
40
41
42
43
44
45
46
47
48
49
50
51
52
53
54
55
56
57
58
59
60
61
62
63
64
65

493 Biosciences, West Heidelberg, Australia) till the turbidity achieved 42% transmittance in a
494 Turbidimeter (Pacificlub, Blackburn, Australia). The cell suspension was then diluted 5 times
495 with IF-0 solution and dye (Cell Biosciences) to final 85% transmittance. BIOLOG PM 1-3
496 (Cell Biosciences, Heidelberg, Australia) were used to investigate the carbon and nitrogen
497 utilisation with two independent biological replicates. Sodium succinate was used as the carbon
498 source for examining nitrogen utilization. Growth was detected after 24-h incubation at 37°C,
499 using an Infinite M200 microplate reader (Tecan, Mannedorf, Switzerland) at 595 nm.
500 Readings that were ≥ 1.5 -fold of the negative control (i.e. growth media without bacteria)
501 indicated the utilisation of nutrients.

502 **Development of a GSMM for *P. aeruginosa* PAO1**

503 To expedite the model development, two curated models for PAO1 with the same identifier
504 systems from Model SEED [32], iMO1056 [28] and Opt20896434 [29] were merged.
505 Databases including KEGG [44], MetaCyc [45], Pseudomonas Genome DB [48] and the
506 literature were employed to complete the model with missing components. The identifiers of
507 metabolites and reactions were kept consistent with Model SEED [29], and cross-referred to
508 MetaCyc, KEGG, PubChem [64], ChEBI [66], ChemSpider [65] and BiGG [67]. The PAO1
509 genome annotation from Pseudomonas Genome DB [48] was employed to construct ‘gene to
510 protein to reaction’ (GPR) associations [91]. A periplasm compartment was incorporated into
511 the model. Reactions and metabolites were then assigned to cytoplasm, periplasm and external
512 environment according to the localisation prediction of metabolic enzymes by PSORTb 3.0
513 [92]. Transport reactions were generated to enable material exchange across membranes
514 according to TCBD [46] and TransporterDB [47]. The model was constructed using the
515 Systems Biology Markup Language (SBML) [93, 94]. VANTED [95] was employed for
516 visualisation and analysis of the metabolic network. For each metabolite in the model, specific
517 features including compartment localisation, mass, charge, formula, formation free energy,

1
2
3
4
5
6
7
8
9
10
11
12
13
14
15
16
17
18
19
20
21
22
23
24
25
26
27
28
29
30
31
32
33
34
35
36
37
38
39
40
41
42
43
44
45
46
47
48
49
50
51
52
53
54
55
56
57
58
59
60
61
62
63
64
65

518 database identifiers and source were added (**Additional file 14**). Each reaction entered into the
519 model was checked with elementary and charge balance. Reversibility was determined first
520 from the primary literature for each particular enzyme or reaction, if available. Further curation
521 on reaction reversibility and directions was conducted based on change of free energy and
522 knowledge about the physiological direction of a reaction in a pathway.

523 The Gapfind function from the COBRA toolbox [96] was employed to identify the isolated and
524 dead-end metabolites in the model. Candidate reactions from KEGG, MetaCyc and BiGG were
525 manually inspected for relevance and homology evidence using BLASTp; reactions catalysed
526 by homologous enzymes (E-value<1×10⁻⁵, identity≥35%, coverage≥50%) were added to the
527 model to eliminate the gaps. Mispredictions of BIOLOG growth phenotypes were employed to
528 refine the draft model (*iPAO1_draft2*). Further curation was performed to represent the
529 complex biosynthesis pathways of macromolecules (e.g. peptidoglycan, GPL and LPS).

530 The biomass formation equation consisting of necessary building blocks for bacterial growth
531 was created using the one from iMO1086 [30], with slight modifications on compositions of
532 ions, peptidoglycans, GPL and LPS (**Additional file 17**). The growth and non-growth
533 associated maintenance was from iMO1086 [30].

534 **Growth prediction in BIOLOG media**

535 *iPAO1* was employed to predict the growth phenotypes on chemically-defined media with 190
536 carbon and 95 nitrogen sources (**Additional file 18**) using the FBA method [24]. The objective
537 function of biomass formation was maximised with the specific nutrient uptake rate set at 10
538 mmol·gDW⁻¹·h⁻¹ under aerobic condition.

$$539 \quad \max \quad v_{\text{biomass}}$$

$$540 \quad s. t. \quad \mathbf{Sv} = 0$$

$$541 \quad a_i \leq v_i \leq b_i, i = 1, 2, \dots, n$$

1
2
3
4
5
6
7
8
9
10
11
12
13
14
15
16
17
18
19
20
21
22
23
24
25
26
27
28
29
30
31
32
33
34
35
36
37
38
39
40
41
42
43
44
45
46
47
48
49
50
51
52
53
54
55
56
57
58
59
60
61
62
63
64
65

542 where v_{biomass} denotes the biomass formation flux, \mathbf{S} represents the stoichiometric matrix and
543 each metabolic flux v_i was constrained by lower and upper bound a_i and b_i , respectively. All
544 modelling procedures were performed with the COBRA toolbox [96] in MATLAB. The
545 calculated specific growth rates v_{biomass} were then compared to the BIOLOG PM data to assess
546 the prediction accuracy using Fisher's exact test.

547 **Gene essentiality prediction**

548 *In silico* single-gene deletion was performed using the CORBRA toolbox and the mutant
549 models were then used to predict the specific growth rate in LB broth [32] using FBA. Genes
550 with 99% reduction of the specific growth rate relative to the wild type were defined as essential
551 for cell growth; otherwise, they were considered as semi-essential (1-99% reduction) and non-
552 essential (<1% reduction). Two existing PAO1 transposon insertion mutant libraries, (i) two-
553 allele mutant library [50, 68] and (ii) mini-Tn5 insertion mutant library [49], were employed
554 to assess the overall prediction accuracy with Fisher's exact test. To determine polymyxin-
555 specific essential genes, transcriptomic constrains were imposed (below) before conducting *in*
556 *silico* single-gene deletion simulations. The calculated essential genes identified in polymyxin
557 treatment alone but not in the control were considered as polymyxin-specific.

558 **Simulation of bacterial growth and metabolic phenotype changes in response to lipid A** 559 **modifications**

560 The LPS stoichiometric coefficients in the biomass formula under the control and lipid A
561 modification conditions were set according to the measured lipid A compositions in the wild-
562 type *P. aeruginosa* PAK and its polymyxin-resistant mutant PAK $_{pmrB6}$, respectively (**Table**
563 **2**) [14]. For PAK $_{pmrB6}$, a missense mutation (L243Q) in *pmrB* resulted in constitutive
564 activation of the PmrAB system and induced expression of the regulated genes regardless of
565 polymyxin, including *arn* operon and *pagL* [42, 97]. Aerobic growth was simulated on minimal

566 media with glucose uptake at $10 \text{ mmol}\cdot\text{gDW}^{-1}\cdot\text{h}^{-1}$. For each simulation, the solution space was
1
2
3 567 sampled with 10,000 random points using the ll-ACHRB algorithm [98]. Flux samples of the
4
5 568 control and lipid A modification were then compared. Significantly perturbed metabolic fluxes
6
7 569 were identified using a Z-score based approach [71].
8
9

10 570 To further analyse the metabolic impact of lipid A modifications, the proportions of all types
11
12 571 of LPS in the biomass formula were randomly assigned and the process was repeated 1,000
13
14 572 times. For each repetition, the specific growth rates were calculated and solution space was
15
16 573 sampled using the methods above. For each type of lipid A, specific physiochemical properties
17
18 574 (*f*) including total atom number, partition coefficient (logP), average charge and molecular
19
20 575 polarity were predicted at pH 7 using the cxcalc tool from ChemAxon (Budapest, Hungary).
21
22
23 576 The overall apparent properties *F* of the OM were estimated by calculating the weighted sum.
24
25
26

$$577 \quad F = \sum_{j=1}^n w_j f_j$$

27
28
29 578 where w_j represents the stoichiometric coefficient of the *j*-th of 288 heterogeneous LPS
30
31 579 molecules in the biomass formula. Pairwise correlation analysis was conducted between lipid
32
33 580 A modifications, physiochemical properties changes, bacterial growth and metabolism
34
35 581 alterations.
36
37
38
39
40
41
42

43 582 **Predict metabolic responses to polymyxin treatment by constraining fluxes with** 44 45 583 **transcriptomics data**

46
47
48
49 584 The RNA-Seq data from 1-h $1 \text{ mg}\cdot\text{L}^{-1}$ polymyxin B treatment experiment using PAO1 were
50
51 585 employed as flux constraints for modelling [51]. For each gene under every condition, the
52
53 586 RPKM (Reads Per Kilobase Million) value was calculated from the aligned reads using the
54
55 587 edgeR package [99], and normalised to constrain flux upper bounds (b_i) using the E-Flux
56
57
58 588 algorithm [26]. Specifically, for each reaction catalysed by a single enzyme, the upper flux
59
60
61
62
63
64
65

589 bound was set to the determined RPKM value under the respective condition. For a reaction
1
2 590 catalysed by an enzyme complex, the upper bound was set to the minimum RPKM value of the
3
4
5 591 associated genes. For a reaction catalysed by isozymes, the upper bound was set to the sum of
6
7 592 RPKM values of the associated genes. The maximum of upper bounds was then normalised to
8
9
10 593 10,000 mmol·gDW⁻¹·h⁻¹. The lower bounds a_i were set to 0 for irreversible and $-b_i$
11
12 594 mmol·gDW⁻¹·h⁻¹ for reversible reactions, respectively. CAMHB was used in the RNA-Seq
13
14
15 595 experiment and it is known as an undefined medium containing mainly amino acids and
16
17 596 oligopeptides [100]. The maximum uptake rates of amino acids in *P. aeruginosa* vary between
18
19
20 597 0.26-1.44 mmol·gDW⁻¹·h⁻¹ [101-103]. Therefore, the upper bounds (b_i^{CAMHB}) of uptake rates
21
22 598 of amino acids, vitamins and dipeptides in *iPAO1* were constrained to 1 mmol·gDW⁻¹·h⁻¹
23
24
25 599 without loss of generality. For each condition, the solution space was sampled with 10,000
26
27 600 points using ll-ACHRB as above. Statistical significance of differential flux distributions was
28
29
30 601 computed using the Z-score method above. The turnover rate for key metabolites was
31
32 602 calculated by summing up all influxes or effluxes [104]. To assess the impact of changing
33
34
35 603 nutrient uptake bounds, sensitivity analysis was conducted by randomly sampling solution
36
37 604 space as above while varying b_i^{CAMHB} from 0.26 to 1.44 mmol·gDW⁻¹·h⁻¹.

40 605

43 606 **Availability of supporting data and materials**

46 607 The raw RNA-Seq data have been deposited in the NCBI Sequence Read Archive (SRA)
47
48
49 608 database under the BioProject accession number PRJNA414673. The metabolomics and
50
51 609 lipidomics data have been deposited in the Metabolight database with the accession number
52
53
54 610 MTBLS630. Supporting data, also including the scripts used in this project, are available via
55
56 611 the *GigaScience* repository GigaDB[106].

59 612

1
2
3 **613 Additional files**

4
5 614 Additional file 1 (additionalFile1.docx): Manual curation of GPL biosynthesis, LPS
6 biosynthesis and modification pathways, and sensitivity analysis of nutrient uptake bounds.

7
8 616 Additional file 2 (additionalFile2.xlsx): Metabolites in the constructed draft model
9 *iPAO1_draft1*.

10
11 617
12
13 618 Additional file 3 (additionalFile3.xlsx): Reactions in the constructed draft model *iPAO1_draft1*.

14
15
16 619 Additional file 4 (additionalFile4.xlsx): Genes in the constructed draft model *iPAO1_draft1*.

17
18
19 620 Additional file 5 (additionalFile5.xlsx). Supplemented metabolites according to previous GC-
20 MS based metabolomics data.
21

22 621
23
24
25 622 Additional file 6 (additionalFile6.xlsx): Supplemented reactions according to previous GS-MS
26 based metabolomics data.
27 623

28
29
30 624 Additional file 7 (additionalFile7.xlsx): Root gap metabolites identified using GapFind from
31 the COBRA toolbox.
32 625

33
34
35 626 Additional file 8 (additionalFile8.xlsx): Comparison of the predicted growth phenotypes with
36 the BIOLOG PM results.
37 627

38
39
40 628 Additional file 9 (additionalFile9.xlsx): Reactions with changed reversibility and directionality
41 during manual curation.
42 629

43
44
45 630 Additional file 10 (additionalFile10.xlsx): Deleted metabolites during manual curation.

46
47 631 Additional file 11 (additionalFile11.xlsx): Deleted reactions during manual curation.

48
49
50 632 Additional file 12 (additionalFile12.xlsx): Added reactions during manual curation.

51
52
53 633 Additional file 13 (additionalFile13.xlsx): Added intermediate metabolites in GPL biosynthesis
54 pathway.
55 634
56
57
58
59
60
61
62
63
64
65

- 1
2
3 635 Additional file 14 (additionalFile14.xlsx): Added reactions in GPL biosynthesis pathway.
4
5
6 636 Additional file 15 (additionalFile15.xlsx): Metabolites in the constructed model *iPAO1*.
7
8
9 637 Additional file 16 (additionalFile16.xlsx): Reactions in the constructed model *iPAO1*.
10
11
12 638 Additional file 17 (additionalFile17.xlsx): Genes in the constructed model *iPAO1*.
13
14
15 639 Additional file 18 (additionalFile18.xlsx): Biomass formation formula.
16
17 640 Additional file 19 (additionalFile19.xlsx): Comparison of the predicted gene essentiality with
18 the information derived from two transposon insertion mutant libraries.
19
20 641 Additional file 20 (additionalFile20.xlsx): Metabolic flux changes in response to lipid A
21 modifications using lipidomics data as stoichiometric constraints.
22
23 642 Additional file 21 (additionalFile21.xlsx): Randomised stoichiometric coefficients of LPS
24 species.
25
26 643 Additional file 22 (additionalFile22.xlsx): Predicted physiochemical properties of lipid A
27 molecules.
28
29 644 Additional file 23 (additionalFile23.xlsx): Metabolic flux changes in response to lipid A
30 modifications with randomly assigned lipid A compositions as stoichiometric constraints.
31
32 645 Additional file 24 (additionalFile24.xlsx): Metabolic flux constraints calculated based on
33 RNA-Seq data.
34
35 646 Additional file 25 (additionalFile25.xlsx): Metabolic flux changes in response to polymyxin
36 treatment using RNA-Seq data as flux constraints.
37
38 647 Additional file 26 (additionalFile26.xlsx): Metabolite turnover rates.
39
40 648 Additional file 27 (additionalFile27.xlsx): Full names of the metabolite abbreviations in Figure
41
42 1.
43
44
45
46
47
48
49
50
51
52
53
54
55
56
57
58
59
60
61
62
63
64
65

657

1
2
3 **658 List of abbreviations**
4

5
6 659 2CS: two-component regulatory system; CAMHB: cation-adjusted Mueller-Hinton broth;
7
8 660 COG: clusters of orthologous groups; FBA: flux balance analysis; FDR: false discovery rate;
9
10 661 GC-MS: gas chromatography-mass spectrometry; GPL: Glycerolphospholipid; GPR: gene to
11
12 662 protein to reaction; GSMM: genome-scale metabolic models; IM: inner membrane; KEGG:
13
14 663 Kyoto Encyclopaedia of Genes and Genomes; L-Ara4N: 4-Amino-4-deoxy-L-arabinose; LB:
15
16 664 Luria-Bertani; LC-MS: liquid chromatography-mass spectrometry; LPS: lipopolysaccharide;
17
18 665 MDR: Multidrug-resistant; OM: outer membrane; PM: Phenotypic Microarray; RPKM: Reads
19
20 666 Per Kilobase Million; SBML: Systems Biology Markup Language; SRA: Sequence Read
21
22 667 Archive; TCDB: Transporter Classification Database.
23
24
25
26
27

28 668
29
30

31 **669 Competing interests**
32

33
34 670 The authors declare no competing interest for this work.
35
36

37 671
38
39

40 **672 Funding**
41

42
43 673 This study was partially supported by a Major Interdisciplinary Research Grant from Monash
44
45 674 University and a project grant by the Australian National Health and Medical Research Council
46
47 675 (NHMRC, APP1127948). J.L., T.V., and J.S. are supported by the National Institute of Allergy
48
49 676 and Infectious Diseases of the National Institutes of Health (R01 AI111965). The content is
50
51 677 solely the responsibility of the authors and does not necessarily represent the official views of
52
53 678 the National Institute of Allergy and Infectious Diseases or the National Institutes of Health.
54
55 679 T.V. is an Australian NHMRC Career Development Research Fellow. T.L. is an Australian
56
57 680 Laureate Fellow supported by Australian Research Council. J.L. is an Australian NHMRC
58
59
60
61
62
63
64
65

681 Senior Research Fellow.

682

683 **Authors' contributions**

684 J.L. and F.S. conceived the project and Y.Z. developed the GSMM and conducted most
685 analysis. T.C. and M.K. validated the model. J.Z., J.Lu and B.S. curated the model. T.V., T.L.
686 and J.S. helped supervise the project. M.H. and M.H.M.M. provided the lipidomics and
687 transcriptomics data, respectively.

688

689 **Acknowledgements**

690 The authors acknowledge the assistance of Dr Darren Creek from the Monash Institute of
691 Pharmaceutical Sciences in LC-MS experiments.

692 **References**

- 1
2
3 693 1. Scales BS, Dickson RP, LiPuma JJ and Huffnagle GB. Microbiology, genomics, and
4
5 694 clinical significance of the *Pseudomonas fluorescens* species complex, an
6
7
8 695 unappreciated colonizer of humans. Clin Microbiol Rev. 2014;27:927-48.
- 9
10 696 2. Breidenstein EB, de la Fuente-Nunez C and Hancock RE. *Pseudomonas aeruginosa*:
11
12 697 all roads lead to resistance. Trends Microbiol. 2011;19:419-26.
- 13
14
15 698 3. Liu YY, Wang Y, Walsh TR, Yi LX, Zhang R, Spencer J, et al. Emergence of plasmid-
16
17 699 mediated colistin resistance mechanism MCR-1 in animals and human beings in China:
18
19
20 700 a microbiological and molecular biological study. Lancet Infect Dis. 2016;16:161-8.
- 21
22 701 4. Winstanley C, O'Brien S and Brockhurst MA. *Pseudomonas aeruginosa* evolutionary
23
24 702 adaptation and diversification in cystic fibrosis chronic lung infections. Trends
25
26
27 703 Microbiol. 2016;24:327-37.
- 28
29
30 704 5. de Almeida Silva KCF, Calomino MA, Deutsch G, de Castilho SR, de Paula GR, Esper
31
32 705 LMR, et al. Molecular characterization of multidrug-resistant (MDR) *Pseudomonas*
33
34 706 *aeruginosa* isolated in a burn center. Burns. 2017;43:137-43.
- 35
36
37 707 6. Church D, Elsayed S, Reid O, Winston B and Lindsay R. Burn wound infections. Clin
38
39 708 Microbiol Rev. 2006;19:403-34.
- 40
41
42 709 7. Klockgether J, Cramer N, Wiehlmann L, Davenport CF and Tummeler B. *Pseudomonas*
43
44 710 *aeruginosa* genomic structure and diversity. Front Microbiol. 2011;2:150.
- 45
46
47 711 8. Ramos JL and Filloux A. *Pseudomonas*: Volume 5: A model system in biology. London:
48
49 712 Springer; 2007.
- 50
51
52 713 9. Nation RL, Li J, Cars O, Couet W, Dudley MN, Kaye KS, et al. Framework for
53
54 714 optimisation of the clinical use of colistin and polymyxin B: the Prato polymyxin
55
56 715 consensus. Lancet Infect Dis. 2015;15:225-34.

- 1
2
3
4
5
6
7
8
9
10
11
12
13
14
15
16
17
18
19
20
21
22
23
24
25
26
27
28
29
30
31
32
33
34
35
36
37
38
39
40
41
42
43
44
45
46
47
48
49
50
51
52
53
54
55
56
57
58
59
60
61
62
63
64
65
- 716 10. Pedersen MG, Jensen-Fangel S, Olesen HV, Nørskov-Lauritsen N and Wang M. 129
717 Colistin resistance in *Achromobacter* sp. and *Pseudomonas aeruginosa* isolated from
718 Danish cystic fibrosis patients is not related to plasmid-mediated expression of *mcr-1*.
719 *J Cyst Fibros.* 2017;16:S98.
- 720 11. Wi YM, Choi JY, Lee JY, Kang CI, Chung DR, Peck KR, et al. Emergence of colistin
721 resistance in *Pseudomonas aeruginosa* ST235 clone in South Korea. *Int J Antimicrob*
722 *Agents.* 2017;49:767-9.
- 723 12. Yu Z, Qin W, Lin J, Fang S and Qiu J. Antibacterial mechanisms of polymyxin and
724 bacterial resistance. *Biomed Res Int.* 2015;2015:679109-19.
- 725 13. Trimble MJ, Mlynarcik P, Kolar M and Hancock RE. Polymyxin: alternative
726 mechanisms of action and resistance. *Cold Spring Harb Perspect Med.* 2016;6:a025288.
- 727 14. Han M, Zhu Y, Cheah SE, Johnson MD, Yu H, Shen HH, et al. Polymyxin resistance
728 in *Pseudomonas aeruginosa*: metabolomic changes underpin lipid A modifications. In:
729 *ASM Microbe 2017* Boston, USA, 2016, p.491.
- 730 15. Hussein MH, Maifiah MHM, Han M, Tran TB, Zhu Y, Hancock REW, et al.
731 Mechanisms of synergistic killing against *Pseudomonas aeruginosa* by polymyxin B
732 and amikacin: A metabolomics study. In: *European Congress of Clinical Microbiology*
733 *and Infectious Diseases* Vienna, Austria, 2017, p.EV0387. ESCMID.
- 734 16. O'Brien EJ, Monk JM and Palsson BO. Using genome-scale models to predict
735 biological capabilities. *Cell.* 2015;161:971-87.
- 736 17. Hohenschuh W, Hector R and Murthy GS. A dynamic flux balance model and
737 bottleneck identification of glucose, xylose, xylulose co-fermentation in
738 *Saccharomyces cerevisiae*. *Bioresour Technol.* 2015;188:153-60.

- 1
2
3
4
5
6
7
8
9
10
11
12
13
14
15
16
17
18
19
20
21
22
23
24
25
26
27
28
29
30
31
32
33
34
35
36
37
38
39
40
41
42
43
44
45
46
47
48
49
50
51
52
53
54
55
56
57
58
59
60
61
62
63
64
65
- 739 18. Hanly TJ and Henson MA. Dynamic metabolic modeling of a microaerobic yeast co-
740 culture: predicting and optimizing ethanol production from glucose/xylose mixtures.
741 Biotechnol Biofuels. 2013;6:44.
- 742 19. Hanly TJ and Henson MA. Dynamic flux balance modeling of microbial co-cultures
743 for efficient batch fermentation of glucose and xylose mixtures. Biotechnol Bioeng.
744 2011;108:376-85.
- 745 20. Bosi E, Monk JM, Aziz RK, Fondi M, Nizet V and Palsson BO. Comparative genome-
746 scale modelling of *Staphylococcus aureus* strains identifies strain-specific metabolic
747 capabilities linked to pathogenicity. Proc Natl Acad Sci U S A. 2016;113:E3801-9.
- 748 21. Kim HU, Kim SY, Jeong H, Kim TY, Kim JJ, Choy HE, et al. Integrative genome-scale
749 metabolic analysis of *Vibrio vulnificus* for drug targeting and discovery. Mol Syst Biol.
750 2011;7:460.
- 751 22. Krueger AS, Munck C, Dantas G, Church GM, Galagan J, Lehar J, et al. Simulating
752 serial-target antibacterial drug synergies using flux balance analysis. PLoS One.
753 2016;11:e0147651.
- 754 23. Aziz RK, Monk JM, Lewis RM, In Loh S, Mishra A, Abhay Nagle A, et al. Systems
755 biology-guided identification of synthetic lethal gene pairs and its potential use to
756 discover antibiotic combinations. Sci Rep. 2015;5:16025.
- 757 24. Bordbar A, Monk JM, King ZA and Palsson BO. Constraint-based models predict
758 metabolic and associated cellular functions. Nat Rev Genet. 2014;15:107-20.
- 759 25. Presta L, Bosi E, Mansouri L, Dijkshoorn L, Fani R and Fondi M. Constraint-based
760 modeling identifies new putative targets to fight colistin-resistant *A. baumannii*
761 infections. Sci Rep. 2017;7:3706.

- 1
2
3
4
5
6
7
8
9
10
11
12
13
14
15
16
17
18
19
20
21
22
23
24
25
26
27
28
29
30
31
32
33
34
35
36
37
38
39
40
41
42
43
44
45
46
47
48
49
50
51
52
53
54
55
56
57
58
59
60
61
62
63
64
65
- 762 26. Colijn C, Brandes A, Zucker J, Lun DS, Weiner B, Farhat MR, et al. Interpreting
763 expression data with metabolic flux models: predicting *Mycobacterium tuberculosis*
764 mycolic acid production. PLoS Comput Biol. 2009;5:e1000489.
- 765 27. Navid A and Almaas E. Genome-level transcription data of *Yersinia pestis* analyzed
766 with a new metabolic constraint-based approach. BMC Syst Biol. 2012;6:150.
- 767 28. Oberhardt MA, Puchalka J, Fryer KE, Martins dos Santos VA and Papin JA. Genome-
768 scale metabolic network analysis of the opportunistic pathogen *Pseudomonas*
769 *aeruginosa* PAO1. J Bacteriol. 2008;190:2790-803.
- 770 29. Henry CS, DeJongh M, Best AA, Frybarger PM, Linsay B and Stevens RL. High-
771 throughput generation, optimization and analysis of genome-scale metabolic models.
772 Nat Biotechnol. 2010;28:977-82.
- 773 30. Oberhardt MA, Puchalka J, Martins dos Santos VA and Papin JA. Reconciliation of
774 genome-scale metabolic reconstructions for comparative systems analysis. PLoS
775 Comput Biol. 2011;7:e1001116.
- 776 31. Bartell JA, Blazier AS, Yen P, Thogersen JC, Jelsbak L, Goldberg JB, et al.
777 Reconstruction of the metabolic network of *Pseudomonas aeruginosa* to interrogate
778 virulence factor synthesis. Nat Commun. 2017;8:14631.
- 779 32. Devoid S, Overbeek R, DeJongh M, Vonstein V, Best AA and Henry C. Automated
780 genome annotation and metabolic model reconstruction in the SEED and Model SEED.
781 Methods Mol Biol. 2013;985:17-45.
- 782 33. Oberhardt MA, Goldberg JB, Hogardt M and Papin JA. Metabolic network analysis of
783 *Pseudomonas aeruginosa* during chronic cystic fibrosis lung infection. J Bacteriol.
784 2010;192:5534-48.
- 785 34. Biggs MB and Papin JA. Novel multiscale modeling tool applied to *Pseudomonas*
786 *aeruginosa* biofilm formation. PLoS One. 2013;8:e78011.

- 787 35. Vital-Lopez FG, Reifman J and Wallqvist A. Biofilm formation mechanisms of
1
2 788 *Pseudomonas aeruginosa* predicted via genome-scale kinetic models of bacterial
3
4 789 metabolism. PLoS Comput Biol. 2015;11:e1004452.
5
6
7 790 36. Sigurdsson G, Fleming RM, Heinken A and Thiele I. A systems biology approach to
8
9 791 drug targets in *Pseudomonas aeruginosa* biofilm. PLoS One. 2012;7:e34337.
10
11 792 37. Xu Z, Fang X, Wood TK and Huang ZJ. A systems-level approach for investigating
12
13 793 *Pseudomonas aeruginosa* biofilm formation. PLoS One. 2013;8:e57050.
14
15
16 794 38. Perumal D, Samal A, Sakharkar KR and Sakharkar MK. Targeting multiple targets in
17
18 795 *Pseudomonas aeruginosa* PAO1 using flux balance analysis of a reconstructed
19
20 796 genome-scale metabolic network. J Drug Target. 2011;19:1-13.
21
22
23 797 39. Dalebroux ZD, Matamouros S, Whittington D, Bishop RE and Miller SI. PhoPQ
24
25 798 regulates acidic glycerophospholipid content of the *Salmonella Typhimurium* outer
26
27 799 membrane. Proc Natl Acad Sci U S A. 2014;111:1963-8.
28
29
30 800 40. Raetz CR, Reynolds CM, Trent MS and Bishop RE. Lipid A modification systems in
31
32 801 Gram-negative bacteria. Annu Rev Biochem. 2007;76:295-329.
33
34
35 802 41. Maifiah MH, Creek DJ, Nation RL, Forrest A, Tsuji BT, Velkov T, et al. Untargeted
36
37 803 metabolomics analysis reveals key pathways responsible for the synergistic killing of
38
39 804 colistin and doripenem combination against *Acinetobacter baumannii*. Sci Rep.
40
41 805 2017;7:45527.
42
43
44 806 42. Han ML, Zhu Y, Cheah S-E, Johnson MD, Yu HH, Maifiah MHM, et al. Polymyxin
45
46 807 resistance due to mutations in *pmrB* caused global metabolomics changes in
47
48 808 *Pseudomonas aeruginosa*. In: *The Australian & New Zealand Metabolomics*
49
50 809 *Conference* Melbourne, Australia, 30 March 2016, p.106.
51
52
53
54
55
56
57
58
59
60
61
62
63
64
65

- 1
2
3
4
5
6
7
8
9
10
11
12
13
14
15
16
17
18
19
20
21
22
23
24
25
26
27
28
29
30
31
32
33
34
35
36
37
38
39
40
41
42
43
44
45
46
47
48
49
50
51
52
53
54
55
56
57
58
59
60
61
62
63
64
65
- 810 43. Frimmersdorf E, Horatzek S, Pelnikevich A, Wiehlmann L and Schomburg D. How
811 *Pseudomonas aeruginosa* adapts to various environments: a metabolomic approach.
812 Environ Microbiol. 2010;12:1734-47.
- 813 44. Kanehisa M, Sato Y, Kawashima M, Furumichi M and Tanabe M. KEGG as a reference
814 resource for gene and protein annotation. Nucleic Acids Res. 2016;44:D457-62.
- 815 45. Caspi R, Billington R, Ferrer L, Foerster H, Fulcher CA, Keseler IM, et al. The
816 MetaCyc database of metabolic pathways and enzymes and the BioCyc collection of
817 pathway/genome databases. Nucleic Acids Res. 2016;44:D471-80.
- 818 46. Saier MH, Jr., Reddy VS, Tsu BV, Ahmed MS, Li C and Moreno-Hagelsieb G. The
819 Transporter Classification Database (TCDB): recent advances. Nucleic Acids Res.
820 2016;44:D372-9.
- 821 47. Elbourne LD, Tetu SG, Hassan KA and Paulsen IT. TransportDB 2.0: a database for
822 exploring membrane transporters in sequenced genomes from all domains of life.
823 Nucleic Acids Res. 2017;45:D320-D4.
- 824 48. Winsor GL, Griffiths EJ, Lo R, Dhillon BK, Shay JA and Brinkman FS. Enhanced
825 annotations and features for comparing thousands of *Pseudomonas* genomes in the
826 *Pseudomonas* genome database. Nucleic Acids Res. 2016;44:D646-53.
- 827 49. Lewenza S, Falsafi RK, Winsor G, Gooderham WJ, McPhee JB, Brinkman FS, et al.
828 Construction of a mini-Tn5-*luxCDABE* mutant library in *Pseudomonas aeruginosa*
829 PAO1: a tool for identifying differentially regulated genes. Genome Res. 2005;15:583-
830 9.
- 831 50. Held K, Ramage E, Jacobs M, Gallagher L and Manoil C. Sequence-verified two-allele
832 transposon mutant library for *Pseudomonas aeruginosa* PAO1. J Bacteriol.
833 2012;194:6387-9.

- 1
2
3
4
5
6
7
8
9
10
11
12
13
14
15
16
17
18
19
20
21
22
23
24
25
26
27
28
29
30
31
32
33
34
35
36
37
38
39
40
41
42
43
44
45
46
47
48
49
50
51
52
53
54
55
56
57
58
59
60
61
62
63
64
65
- 834 51. Maifiah MHM. *Deciphering the modes of action of polymyxins and the synergistic*
835 *combinations against multidrug-resistant Gram-negative bacteria: a systems*
836 *pharmacology approach*. PhD thesis, Monash University, Australia, 2017.
- 837 52. Liao Y, Smyth GK and Shi W. The Subread aligner: fast, accurate and scalable read
838 mapping by seed-and-vote. *Nucleic Acids Res.* 2013;41:e108.
- 839 53. Powell D: Degust. <http://degust.erc.monash.edu/> (2017). Accessed Oct 18 2017.
- 840 54. Creek DJ, Jankevics A, Burgess KE, Breitling R and Barrett MP. IDEOM: an Excel
841 interface for analysis of LC-MS-based metabolomics data. *Bioinformatics.*
842 2012;28:1048-9.
- 843 55. Satish Kumar V, Dasika MS and Maranas CD. Optimization based automated curation
844 of metabolic reconstructions. *BMC Bioinformatics.* 2007;8:212.
- 845 56. Finn RD, Coghill P, Eberhardt RY, Eddy SR, Mistry J, Mitchell AL, et al. The Pfam
846 protein families database: towards a more sustainable future. *Nucleic Acids Res.*
847 2016;44:D279-85.
- 848 57. Zdobnov EM, Tegenfeldt F, Kuznetsov D, Waterhouse RM, Simao FA, Ioannidis P, et
849 al. OrthoDB v9.1: cataloging evolutionary and functional annotations for animal,
850 fungal, plant, archaeal, bacterial and viral orthologs. *Nucleic Acids Res.* 2017;45:D744-
851 D9.
- 852 58. Hempel N, Görisch H and Mern DS. Gene *ercA*, encoding a putative iron-containing
853 alcohol dehydrogenase, is involved in regulation of ethanol utilization in *Pseudomonas*
854 *aeruginosa*. *J Bacteriol.* 2013;195:3925-32.
- 855 59. Kohanski MA, Dwyer DJ and Collins JJ. How antibiotics kill bacteria: from targets to
856 networks. *Nat Rev Microbiol.* 2010;8:423-35.
- 857 60. Typas A, Banzhaf M, Gross CA and Vollmer W. From the regulation of peptidoglycan
858 synthesis to bacterial growth and morphology. *Nat Rev Microbiol.* 2011;10:123-36.

- 1
2
3
4
5
6
7
8
9
10
11
12
13
14
15
16
17
18
19
20
21
22
23
24
25
26
27
28
29
30
31
32
33
34
35
36
37
38
39
40
41
42
43
44
45
46
47
48
49
50
51
52
53
54
55
56
57
58
59
60
61
62
63
64
65
- 859 61. Cox E, Michalak A, Pagentine S, Seaton P and Pokorny A. Lysylated phospholipids
860 stabilize models of bacterial lipid bilayers and protect against antimicrobial peptides.
861 Biochim Biophys Acta. 2014;1838:2198-204.
- 862 62. Kondakova T, D'Heygere F, Feuilloley MJ, Orange N, Heipieper HJ and Duclairoir Poc
863 C. Glycerophospholipid synthesis and functions in *Pseudomonas*. Chem Phys Lipids.
864 2015;190:27-42.
- 865 63. Velkov T, Thompson PE, Nation RL and Li J. Structure–activity relationships of
866 polymyxin antibiotics. J Med Chem. 2010;53:1898-916.
- 867 64. Kim S, Thiessen PA, Bolton EE, Chen J, Fu G, Gindulyte A, et al. PubChem Substance
868 and Compound databases. Nucleic Acids Res. 2016;44:D1202-13.
- 869 65. Pence HE and Williams A. ChemSpider: an online chemical information resource. J
870 Chem Educ. 2010;87:1123-4.
- 871 66. Hastings J, de Matos P, Dekker A, Ennis M, Harsha B, Kale N, et al. The ChEBI
872 reference database and ontology for biologically relevant chemistry: enhancements for
873 2013. Nucleic Acids Res. 2013;41:D456-63.
- 874 67. King ZA, Lu J, Drager A, Miller P, Federowicz S, Lerman JA, et al. BiGG Models: A
875 platform for integrating, standardizing and sharing genome-scale models. Nucleic
876 Acids Res. 2016;44:D515-22.
- 877 68. Jacobs MA, Alwood A, Thaipisuttikul I, Spencer D, Haugen E, Ernst S, et al.
878 Comprehensive transposon mutant library of *Pseudomonas aeruginosa*. Proc Natl Acad
879 Sci U S A. 2003;100:14339-44.
- 880 69. Gutu AD, Sgambati N, Strasbourger P, Brannon MK, Jacobs MA, Haugen E, et al.
881 Polymyxin resistance of *Pseudomonas aeruginosa* *phoQ* mutants is dependent on
882 additional two-component regulatory systems. Antimicrob Agents Chemother.
883 2013;57:2204-15.

- 884 70. Olaitan AO, Morand S and Rolain JM. Mechanisms of polymyxin resistance: acquired
1 and intrinsic resistance in bacteria. *Front Microbiol.* 2014;5:643.
2 885
3
4 886 71. Mo ML, Palsson BO and Herrgard MJ. Connecting extracellular metabolomic
5 measurements to intracellular flux states in yeast. *BMC Syst Biol.* 2009;3:37.
6 887
7
8 888 72. Graham LL, Beveridge TJ and Nanninga N. Periplasmic space and the concept of the
9 periplasm. *Trends Biochem Sci.* 1991;16:328-9.
10 889
11
12 890 73. Silhavy TJ, Kahne D and Walker S. The bacterial cell envelope. *Cold Spring Harb*
13 *Perspect Biol.* 2010;2:a000414.
14 891
15
16 892 74. Han M, Shen HH, Zhu Y, Roberts KD, Le Brun AP, Moskowitz SM, et al. Deciphering
17 the mechanisms of polymyxin resistance in *Pseudomonas aeruginosa*: A systems
18 pharmacology and neutron reflectometry approach. In: *Solutions for Drug-Resistant*
19 *Infections (SDRI) 2017* Brisbane, Australia, 3-5, April 2017, p.P23. SDRI 2017.
20 893
21
22 894
23
24 895
25
26 896 75. Maifiah MH, Cheah SE, Johnson MD, Han ML, Boyce JD, Thamlikitkul V, et al.
27 Global metabolic analyses identify key differences in metabolite levels between
28 polymyxin-susceptible and polymyxin-resistant *Acinetobacter baumannii*. *Sci Rep.*
29 2016;6:22287.
30 897
31
32 898
33
34 899
35
36 900 76. Henry R, Crane B, Powell D, Deveson Lucas D, Li Z, Aranda J, et al. The
37 transcriptomic response of *Acinetobacter baumannii* to colistin and doripenem alone
38 and in combination in an *in vitro* pharmacokinetics/pharmacodynamics model. *J*
39 *Antimicrob Chemother.* 2015;70:1303-13.
40 901
41
42 902
43
44 903
45
46 904 77. Abdul Rahim N, Cheah S, Zhu Y, Johnson M, Boyce J, Yu H, et al. Integrative multi-
47 omics network analysis of the synergistic killing of polymyxin B and chloramphenicol
48 combination against an NDM-producing *Klebsiella pneumoniae* isolate. In: *2016*
49 *European Congress of Clinical Microbiology and Infectious Diseases (ECCMID)*
50 *Amsterdam, Netherland, 2016, p.EV0651. ESCMID.*
51 905
52
53 906
54
55 907
56
57 908
58
59
60
61
62
63
64
65

- 1
2
3
4
5
6
7
8
9
10
11
12
13
14
15
16
17
18
19
20
21
22
23
24
25
26
27
28
29
30
31
32
33
34
35
36
37
38
39
40
41
42
43
44
45
46
47
48
49
50
51
52
53
54
55
56
57
58
59
60
61
62
63
64
65
- 909 78. Machado D and Herrgard M. Systematic evaluation of methods for integration of
910 transcriptomic data into constraint-based models of metabolism. PLoS Comput Biol.
911 2014;10:e1003580.
- 912 79. Blazier AS and Papin JA. Integration of expression data in genome-scale metabolic
913 network reconstructions. Front Physiol. 2012;3:299.
- 914 80. Segre D, Vitkup D and Church GM. Analysis of optimality in natural and perturbed
915 metabolic networks. Proc Natl Acad Sci U S A. 2002;99:15112-7.
- 916 81. Kohanski MA, Dwyer DJ, Hayete B, Lawrence CA and Collins JJ. A common
917 mechanism of cellular death induced by bactericidal antibiotics. Cell. 2007;130:797-
918 810.
- 919 82. Johnson L, Mulcahy H, Kanevets U, Shi Y and Lewenza S. Surface-localized
920 spermidine protects the *Pseudomonas aeruginosa* outer membrane from antibiotic
921 treatment and oxidative stress. J Bacteriol. 2012;194:813-26.
- 922 83. Fernandez L, Jenssen H, Bains M, Wiegand I, Gooderham WJ and Hancock RE. The
923 two-component system CprRS senses cationic peptides and triggers adaptive resistance
924 in *Pseudomonas aeruginosa* independently of ParRS. Antimicrob Agents Chemother.
925 2012;56:6212-22.
- 926 84. Barrow K and Kwon DH. Alterations in two-component regulatory systems of *phoPQ*
927 and *pmrAB* are associated with polymyxin B resistance in clinical isolates of
928 *Pseudomonas aeruginosa*. Antimicrob Agents Chemother. 2009;53:5150-4.
- 929 85. Owusu-Anim D and Kwon DH. Differential role of two-component regulatory systems
930 (*phoPQ* and *pmrAB*) in polymyxin B susceptibility of *Pseudomonas aeruginosa*. Adv
931 Microbiol. 2012;2:31-6.

- 1
2
3
4
5
6
7
8
9
10
11
12
13
14
15
16
17
18
19
20
21
22
23
24
25
26
27
28
29
30
31
32
33
34
35
36
37
38
39
40
41
42
43
44
45
46
47
48
49
50
51
52
53
54
55
56
57
58
59
60
61
62
63
64
65
- 932 86. Moskowitz SM, Ernst RK and Miller SI. PmrAB, a two-component regulatory system
933 of *Pseudomonas aeruginosa* that modulates resistance to cationic antimicrobial
934 peptides and addition of aminoarabinose to lipid A. J Bacteriol. 2004;186:575-9.
- 935 87. Winfield MD and Groisman EA. Phenotypic differences between *Salmonella* and
936 *Escherichia coli* resulting from the disparate regulation of homologous genes. Proc Natl
937 Acad Sci U S A. 2004;101:17162-7.
- 938 88. McPhee JB, Bains M, Winsor G, Lewenza S, Kwasnicka A, Brazas MD, et al.
939 Contribution of the PhoP-PhoQ and PmrA-PmrB two-component regulatory systems to
940 Mg²⁺-induced gene regulation in *Pseudomonas aeruginosa*. J Bacteriol.
941 2006;188:3995-4006.
- 942 89. Thaipisuttikul I, Hittle LE, Chandra R, Zangari D, Dixon CL, Garrett TA, et al. A
943 divergent *Pseudomonas aeruginosa* palmitoyltransferase essential for cystic fibrosis-
944 specific lipid A. Mol Microbiol. 2014;91:158-74.
- 945 90. Fernández L, Gooderham WJ, Bains M, McPhee JB, Wiegand I and Hancock REW.
946 Adaptive resistance to the “last hope” antibiotics polymyxin B and colistin in
947 *Pseudomonas aeruginosa* is mediated by the novel two-component regulatory system
948 ParR-ParS. Antimicrob Agents Chemother. 2010;54:3372-82.
- 949 91. Thiele I and Palsson BO. A protocol for generating a high-quality genome-scale
950 metabolic reconstruction. Nat Protoc. 2010;5:93-121.
- 951 92. Yu NY, Wagner JR, Laird MR, Melli G, Rey S, Lo R, et al. PSORTb 3.0: improved
952 protein subcellular localization prediction with refined localization subcategories and
953 predictive capabilities for all prokaryotes. Bioinformatics. 2010;26:1608-15.
- 954 93. Hucka M, Finney A, Sauro HM, Bolouri H, Doyle JC, Kitano H, et al. The systems
955 biology markup language (SBML): a medium for representation and exchange of
956 biochemical network models. Bioinformatics. 2003;19:524-31.

- 1
2
3
4
5
6
7
8
9
10
11
12
13
14
15
16
17
18
19
20
21
22
23
24
25
26
27
28
29
30
31
32
33
34
35
36
37
38
39
40
41
42
43
44
45
46
47
48
49
50
51
52
53
54
55
56
57
58
59
60
61
62
63
64
65
- 957 94. Hucka M and Finney AM: Systems Biology Markup Language (SBML) Level 2:
958 Structures and Facilities for Model Definitions.
959 <http://identifiers.org/combine.specifications/sbml.level-2.version-1> (2003). Accessed
960 Oct 18 2017.
- 961 95. Rohn H, Junker A, Hartmann A, Grafahrend-Belau E, Treutler H, Klapperstuck M, et
962 al. VANTED v2: a framework for systems biology applications. BMC Syst Biol.
963 2012;6:139.
- 964 96. Schellenberger J, Que R, Fleming RM, Thiele I, Orth JD, Feist AM, et al. Quantitative
965 prediction of cellular metabolism with constraint-based models: the COBRA Toolbox
966 v2.0. Nat Protoc. 2011;6:1290-307.
- 967 97. Moskowitz SM, Brannon MK, Dasgupta N, Pier M, Sgambati N, Miller AK, et al. PmrB
968 mutations promote polymyxin resistance of *Pseudomonas aeruginosa* isolated from
969 colistin-treated cystic fibrosis patients. Antimicrob Agents Chemother. 2012;56:1019-
970 30.
- 971 98. Saa PA and Nielsen LK. Il-ACHRB: a scalable algorithm for sampling the feasible
972 solution space of metabolic networks. Bioinformatics. 2016;32:2330-7.
- 973 99. McCarthy DJ, Chen Y and Smyth GK. Differential expression analysis of multifactor
974 RNA-Seq experiments with respect to biological variation. Nucleic Acids Res.
975 2012;40:4288-97.
- 976 100. Mueller JH and Hinton J. A protein-free medium for primary isolation of the
977 *Gonococcus* and Meningococcus. Proc Soc Exp Biol Med. 1941;48:330-3.
- 978 101. Hoshino T. Transport systems for branched-chain amino acids in *Pseudomonas*
979 *aeruginosa*. J Bacteriol. 1979;139:705-12.
- 980 102. Yoshimura F and Nikaido H. Permeability of *Pseudomonas aeruginosa* outer
981 membrane to hydrophilic solutes. J Bacteriol. 1982;152:636-42.

- 982 103. Kay WW and Gronlund AF. Transport of aromatic amino acids by *Pseudomonas*
1
2 983 *aeruginosa*. J Bacteriol. 1971;105:1039-46.
3
4 984 104. Kim PJ, Lee DY, Kim TY, Lee KH, Jeong H, Lee SY, et al. Metabolite essentiality
5
6 elucidates robustness of *Escherichia coli* metabolism. Proc Natl Acad Sci U S A.
7 985
8
9 986 2007;104:13638-42.
10
11 987 105. Benjamini Y and Hochberg Y. Controlling the false discovery rate: A practical and
12
13 powerful approach to multiple testing. J Roy Stat Soc B Met. 1995;57:289-300.
14 988
15
16 989 106. Zhu Y, Czauderna T, Zhao J, Klapperstueck M, Maifiah MH, Han ML et al. Supporting
17
18 data for "Genome-scale metabolic modelling of responses to polymyxins in
19 990
20
21 Pseudomonas aeruginosa." *Gigascience Database* 2018.
22 991
23
24 992 <http://dx.doi.org/10.5524/100414>
25
26 993
27
28

994 **Figure legends**

995 **Figure 1.** The curated GPL biosynthesis in *iPAO1*. [c], intracellular metabolites; [p],
996 periplasmic metabolites; [e], external metabolites. Blue arrows indicate transport reactions.

997 Full names of metabolite classes are listed in **Additional file 27**.

998 **Figure 2.** LPS biosynthesis and modification in *iPAO1*. (A) VANTED diagram showing the
999 biosynthesis of different LPS molecules. (B) LPS biosynthesis pathway; lipid A and LPS are
1000 indicated in the same colour as in (A).

1001 **Figure 3.** Constitutional genes, reactions and metabolites in *iPAO1*. (A) Sources of *iPAO1*
1002 components. (B) Radar map showing the percentages of metabolites and reactions with valid
1003 database identifiers. (C) The COG functional classification of the involved genes in iMO1056,
1004 Opt208964 and *iPAO1*. Percentages given in the middle indicate the coverages of COG groups.
1005 The proportions of the curated reactions (D), reaction-to-gene ratio (E) and predicted

1006 subcellular localisations of the involved proteins (F) are shown for each pathway or COG group.
1
21007 In panel D, red bars indicate the curated reactions; whereas blue bars indicate the reactions
3
4
51008 from previous model. In panel D and E, pathways with the highest curation proportion or
6
71009 reaction-to-gene ratio are highlighted in red.
8
9
101010 **Figure 4.** Comparison of the BIOLOG result (left columns) and model prediction (right
11
12
131011 columns). Blue indicates growth; whereas yellow indicates no growth.
14
15
161012 **Figure 5.** Simulation of the impact of lipid A modifications on bacterial growth, metabolism
17
181013 and OM physiochemical properties. The significant correlation ($P<0.05$) of paired items is
19
201014 indicated in red.
21
22
231015 **Figure 6.** Polymyxin B induced metabolic perturbations. The distributions of metabolic fluxes
24
25
261016 and metabolite turnover rates are shown in subgraphs with red indicating control and blue
27
281017 indicating polymyxin B treatment.
29
30
311018 **Figure S1.** Sensitivity analysis of the mean metabolic fluxes (A) and metabolite turnover rates
32
33
341019 to the variation of nutrient uptake upper bounds. Red indicates the control and blue indicates
35
361020 polymyxin B treatment.
37
38
391021
40
41
421022
43
44
45
46
47
48
49
50
51
52
53
54
55
56
57
58
59
60
61
62
63
64
65

1023 **Tables and their legends**

1
2
3
4
5
6
7
8
9
10
11
12
13
14
15
16
17
18
19
20
21
22
23
24
25
26
27
28
29
30
31
32
33
34
35
36
37
38
39
40
41
42
43
44
45
46
47
48
49
50
51
52
53
54
55
56
57
58
59
60
61
62
63
64
65

1024 **Table 1.** Components in model iMO1056, Opt208964 and iPAO1.

	<i>iPAO1</i>	<i>iMO1056</i>	<i>Opt208964</i>
Genes	1,458	1,042	1,021
Reactions	4,365	992	1,609
Cytoplasmic metabolic reactions	1,716	730	1,132
Periplasmic metabolic reactions	403	0	0
External metabolic reactions	40	0	0
Transport reactions	960	150	253
Transport across IM	519	0	0
Transport across OM	441	0	0
Transport from cytoplasm to extracellular space	0	150	253
Boundary reactions	352	112	223
Reactions without associated genes	628	159	374
Sink reactions	0	0	1
Metabolites	3,022	858	1,344
Cytosol	1,519	746	1,121
Periplasm	698	0	0
Extracellular space	805	112	223

1
2
3
4
5
6
7
8
9
10
11
12
13
14
15
16
17
18
19
20
21
22
23
24
25
26
27
28
29
30
31
32
33
34
35
36
37
38
39
40
41
42
43
44
45
46
47
48
49
50
51
52
53
54
55
56
57
58
59
60
61
62
63
64
65

^a Pathway information is not available in iMO1056 from the Model SEED database.

1027 **Table 2.** Lipid A composition (%) in the outer leaflet of the OM in PAO1 [14].

Lipid A species	Control	Polymyxin B treated
Hexa-lipid A	42.5±0.46	11.7±1.13
Penta-lipid A	57.5±0.46	67.7±3.16
L-Aminoarabinosylated hexa-LA	0	1.24±0.31
L-Aminoarabinosylated penta-LA	0	19.4±3.44
Total	100	100

1
2
3
4
5
6
7
8
9
10
11
12
13
14
15
16
17
18
19
20
21
22
23
24
25
26
27
28
29
30
31
32
33
34
35
36
37
38
39
40
41
42
43
44
45
46
47
48
49
50
51
52
53
54
55
56
57
58
59
60
61
62
63
64
65

1028

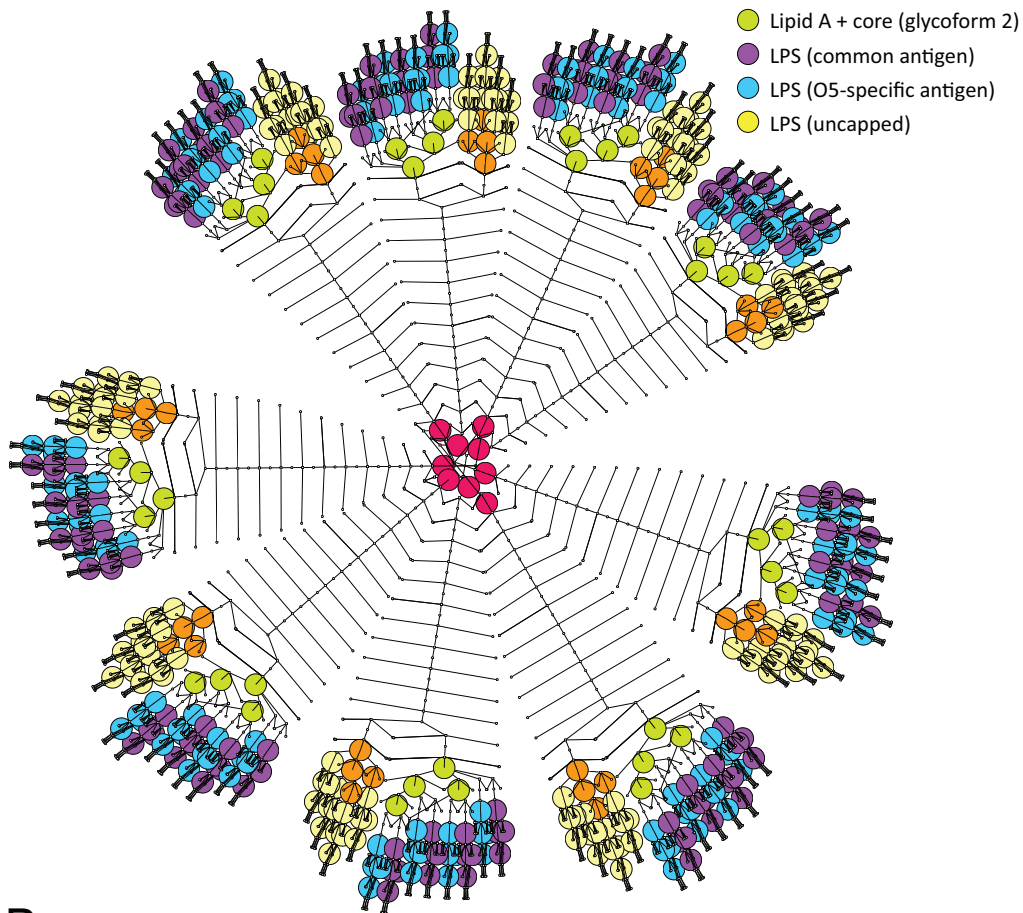
1029

1030 **Table 3.** Specific growth rate, significantly altered major exchange fluxes (>1 mmol·gDW⁻¹·h⁻¹), respiration quotient and the fluxes through F₀F₁-ATPase calculated using the RNA-Seq
 1031 data [51] as flux constraints.
 1032

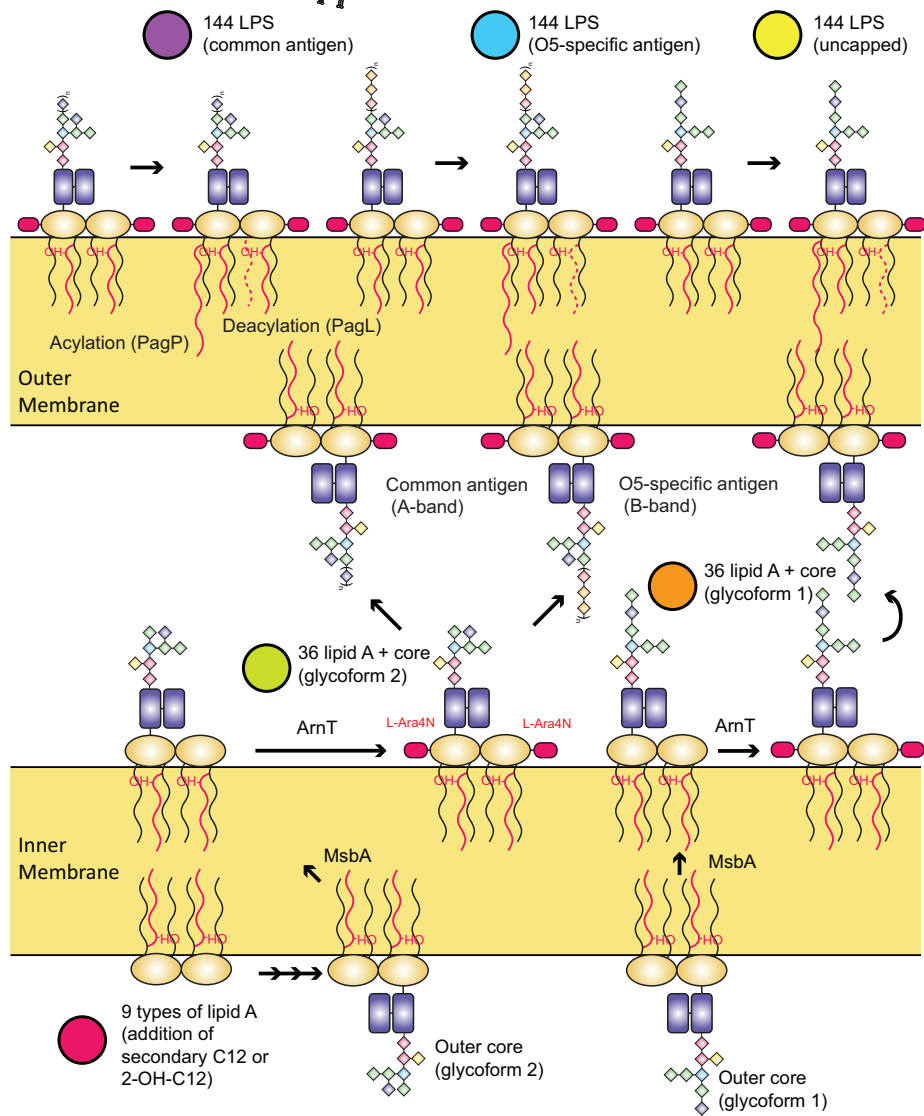
Exchange flux (mmol·gDW ⁻¹ ·h ⁻¹)	Control	Polymyxin B treatment	Z-score	FDR ^a
Specific growth rate (h ⁻¹)	0.82±0.00	0.67±0.00	10,201.3	0.00
H ₂ O	46.9±21.8	53.0±19.0	20.37	0.00
O ₂	-106.0±23.0	-113.4±19.8	24.30	0.00
CO ₂	109.2±22.6	115.8±19.3	22.62	0.00
NH ₄ ⁺	36.6±9.29	38.0±8.77	10.94	0.00
Glycine	2.15±4.76	1.92±4.46	3.05	0.00
L-Alanine	1.21±5.01	-0.52±2.20	31.77	0.00
Succinate	2.08±4.19	2.52±4.42	7.27	0.00
H ⁺	-41.5±14.1	-40.4±11.9	6.44	0.00
Methanethiol	1.53±0.82	1.34±1.11	12.62	0.00
H ₂ S	1.66±1.74	1.41±2.18	9.29	0.00
Respiration Quotient (RQ)	1.03±0.10	1.02±0.10	7.63	0.00
ATPase (mmol·gDW ⁻¹ ·h ⁻¹)	-188.6±52.4	-167.6±48.4	29.62	0.00

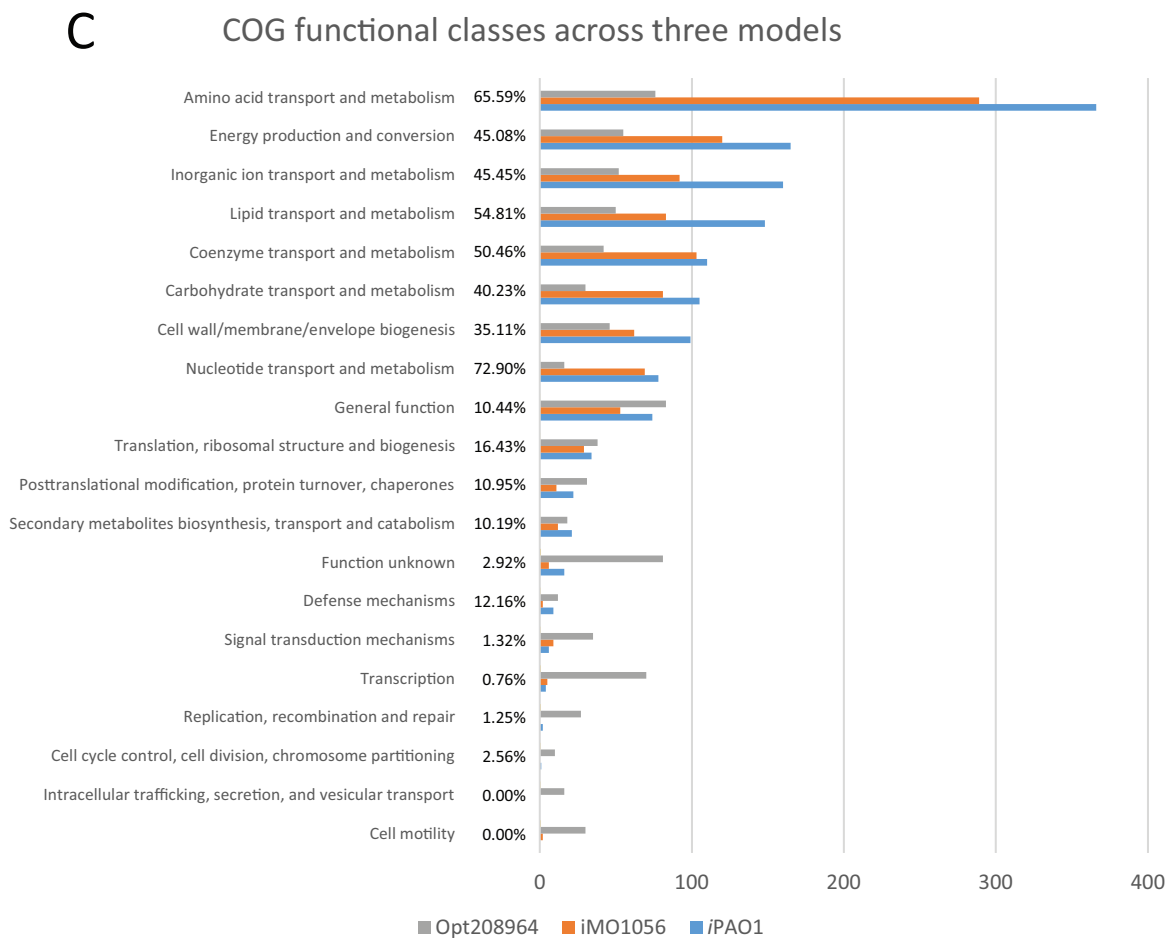
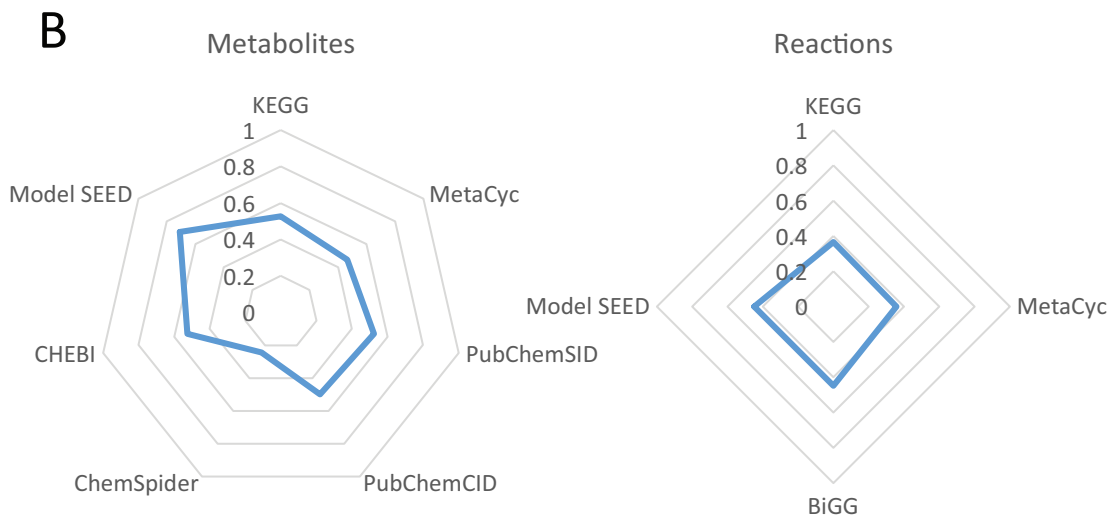
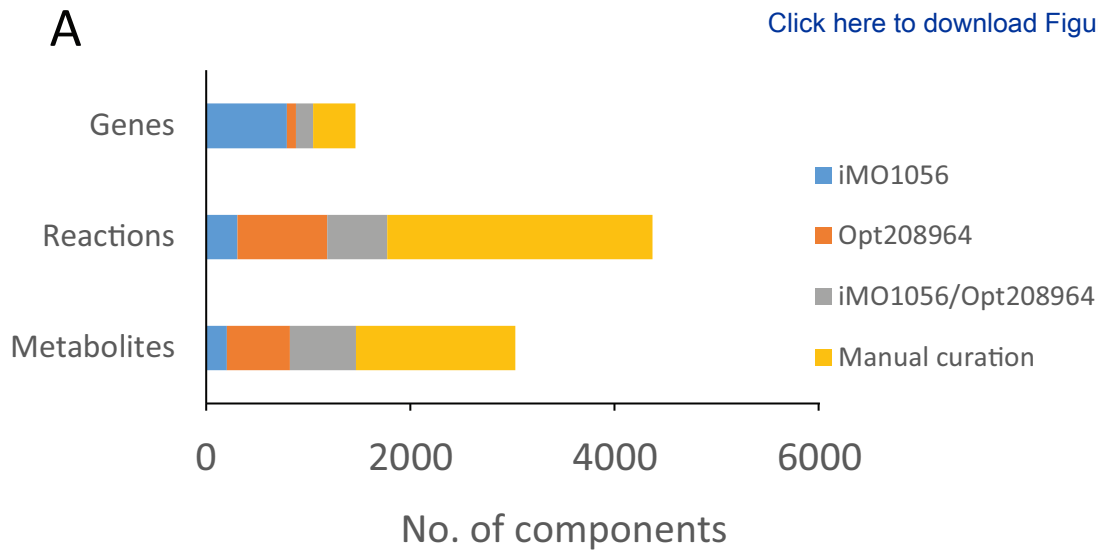
^a FDR was calculated using the Benjamini-Hochberg method [105].

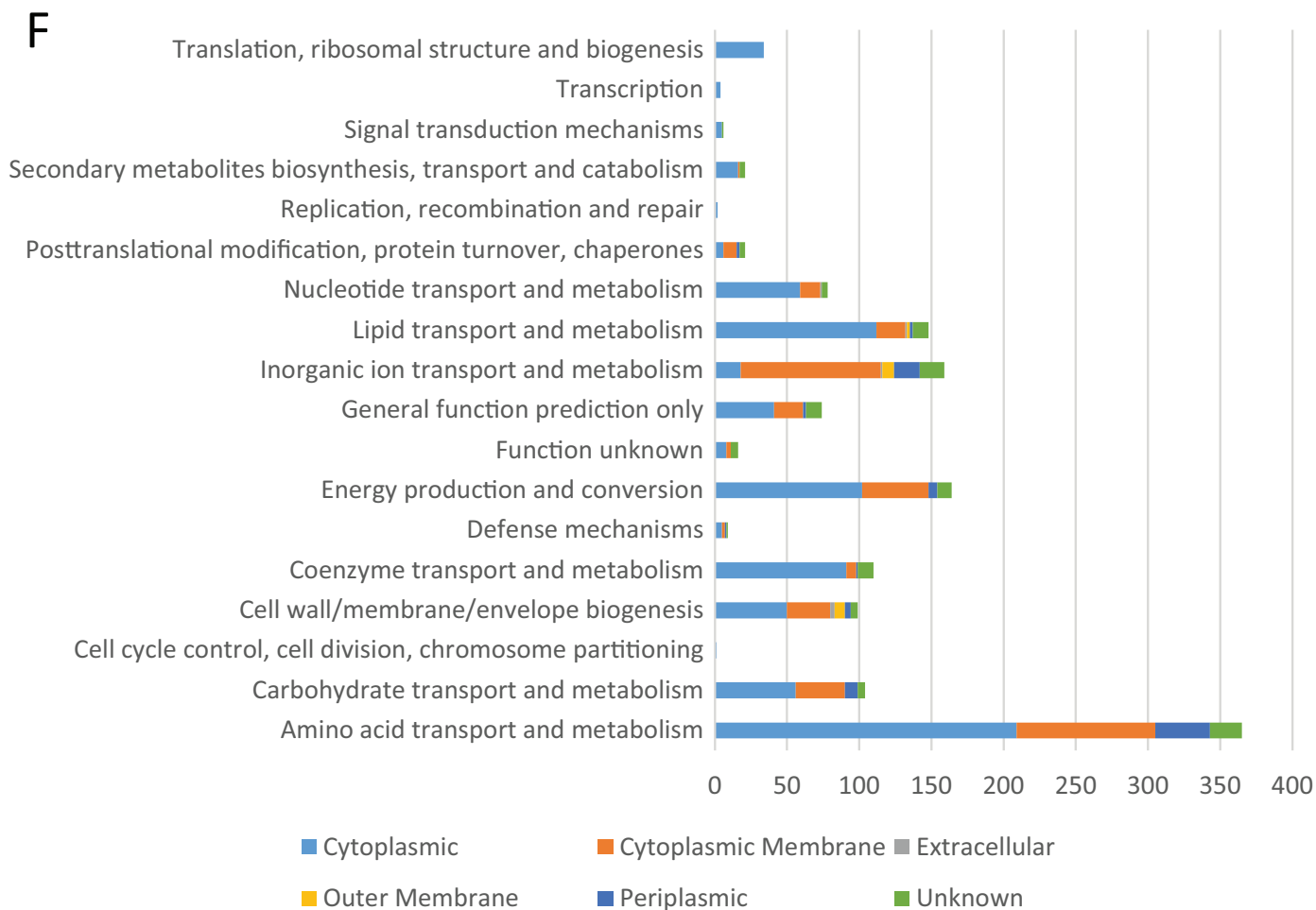
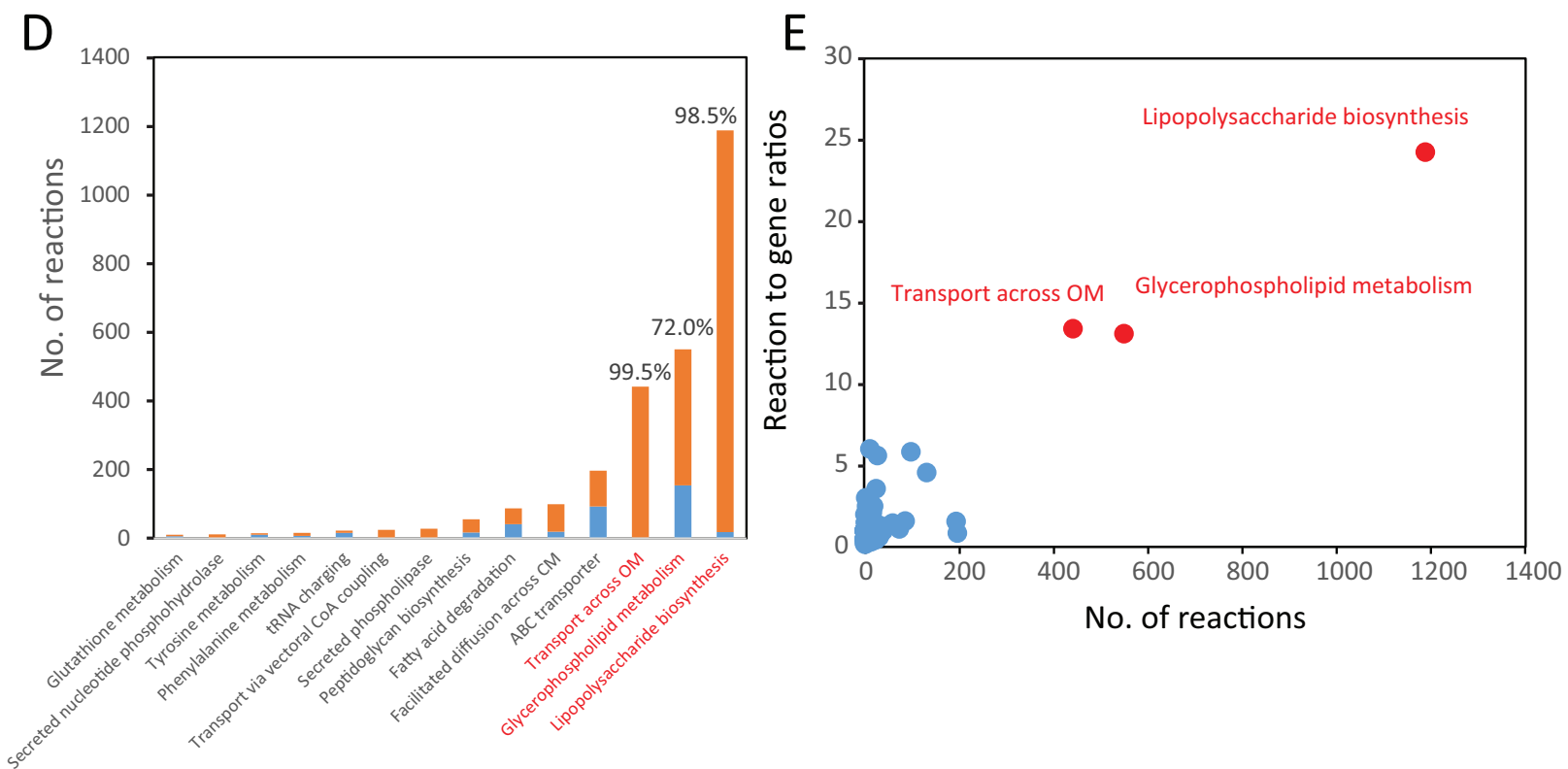
1034



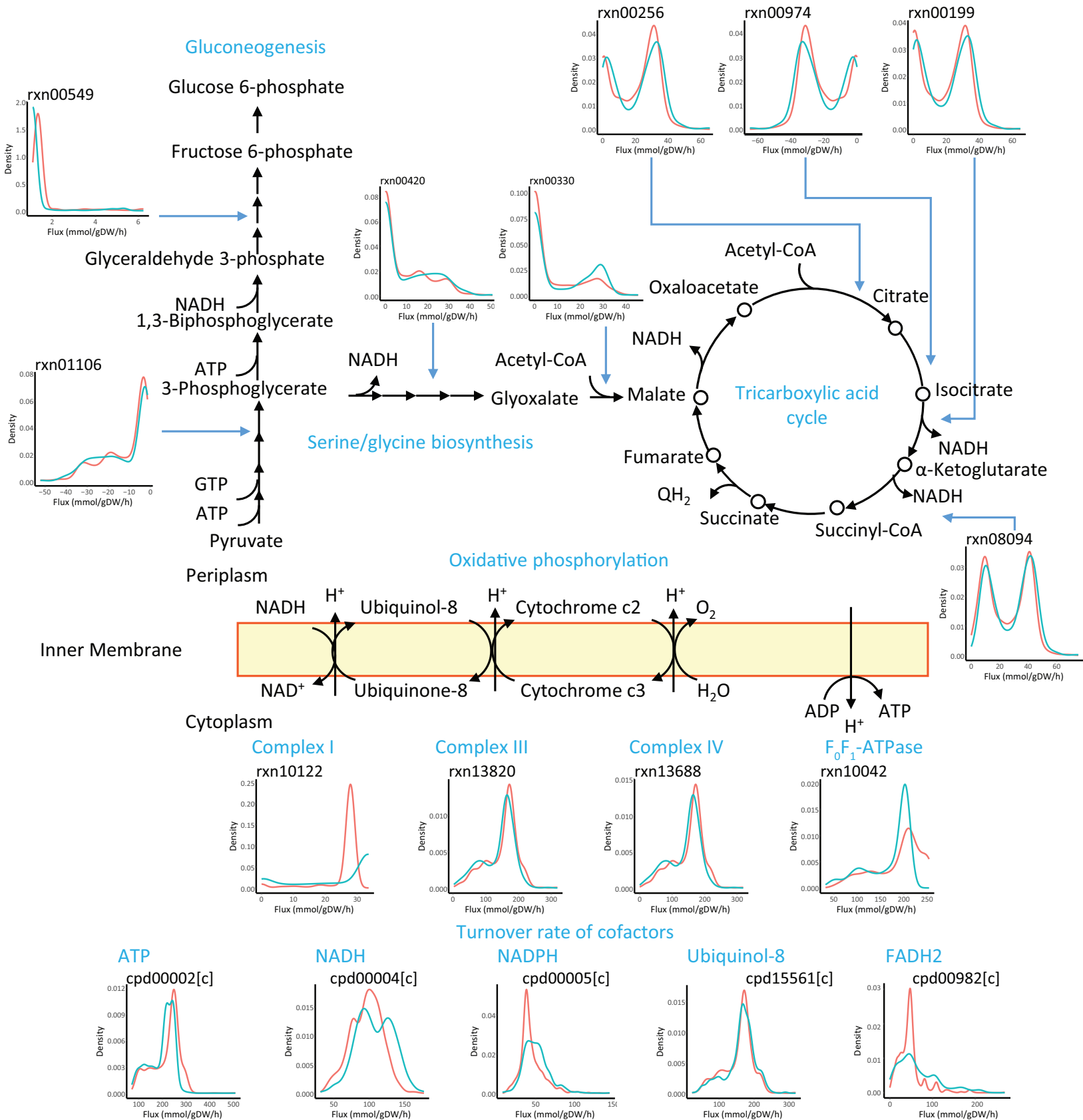
B

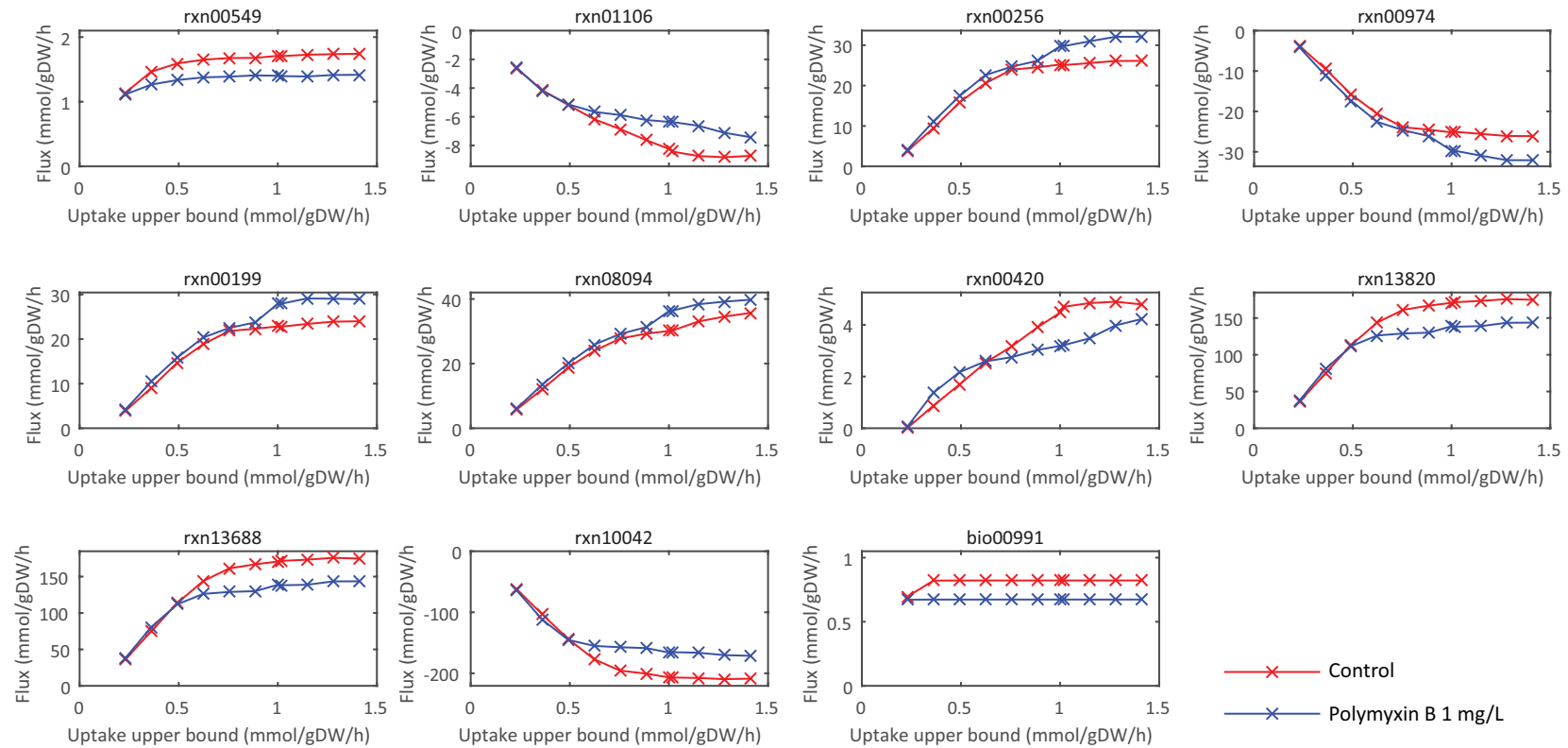
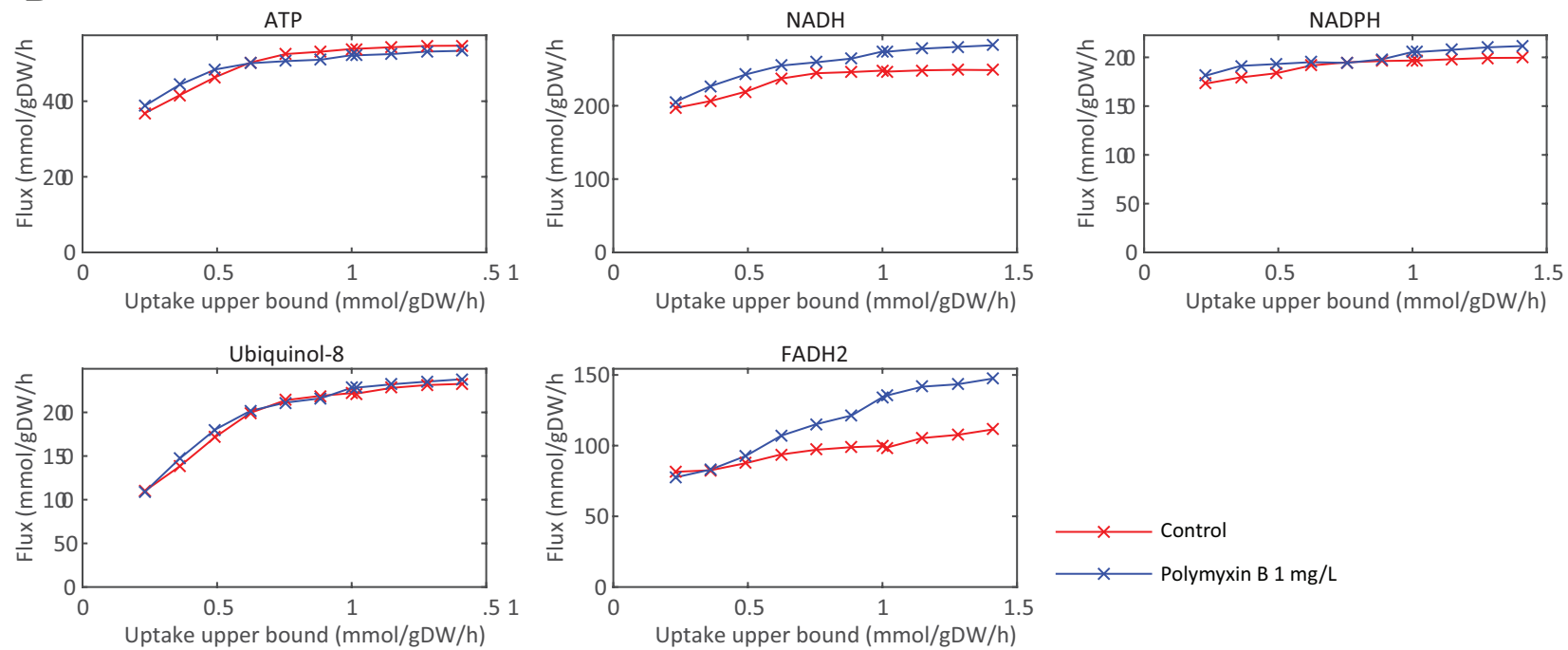







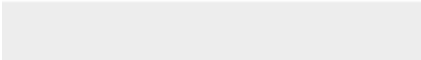

PM1 (Carbon)	Biolog /PAO1	PM2 (Carbon)	Biolog /PAO1	PM3 (Nitrogen)	Biolog /PAO1			
L-Arabinose	x	x	Chondroitin Sulfate C	x	x	Ammonia	v	v
N-Acetyl-D-Glucosamine	v	v	a-Cyclodextrin	x	x	Nitrite	v	v
D-Saccharic Acid	x	x	b-Cyclodextrin	x	x	Sodium Nitrate	v	v
Succinic Acid	v	v	g-Cyclodextrin	x	x	Urea	v	v
D-Galactose	x	x	Dextrin	x	x	Biuret	x	x
L-Aspartic Acid	v	v	Gelatin	x	x	L-Alanine	v	v
L-Proline	v	v	Glycogen	x	x	L-Arginine	v	v
D-Alanine	v	v	Inulin	x	x	L-Asparagine	v	v
D-Trehalose	x	v	Laminarin	x	x	L-Aspartic Acid	v	v
D-Mannose	x	x	Mannan	x	x	L-Cysteine	v	v
Dulcitol	x	x	Pectin	x	x	L-Glutamic Acid	v	v
D-Serine	x	v	N-Acetyl-D-Galactosamine	x	x	L-Glutamine	v	v
D-Sorbitol	x	x	N-Acetyl-Neuraminic Acid	x	x	Glycine	v	v
Glycerol	v	v	b-D-Allose	x	x	L-Histidine	v	v
L-Fucose	x	x	D-Amygdalin	x	x	L-Isoleucine	v	v
D-Glucuronic Acid	x	x	D-Arabinose	x	x	L-Leucine	v	v
D-Gluconic Acid	v	v	D-Arabitol	x	x	L-Lysine	v	v
D,L-a-Glycerol Phosphate	x	v	L-Arabitol	x	x	L-Methionine	v	v
D-Xylose	x	x	Arbutin	x	x	L-Phenylalanine	v	v
L-Lactic Acid	v	v	2-Deoxy-D-Ribose	x	x	L-Proline	v	v
Formic Acid	v	v	i-Erythritol	x	x	L-Serine	v	v
D-Mannitol	v	v	D-Fucose	x	x	L-Threonine	v	v
L-Glutamic Acid	v	v	3-0-b-D-Galacto-pyranosyl-D-Arabinose	x	x	L-Tryptophan	v	v
D-Glucose-6-Phosphate	x	v	Gentobiose	x	x	L-Tyrosine	v	v
D-Galactonic Acid-g-Lactone	x	x	L-Glucose	x	x	L-Valine	v	v
D,L-Malic Acid	v	v	Lactitol	x	x	D-Alanine	v	v
D-Ribose	v	v	D-Melezitose	x	x	D-Asparagine	v	v
Tween 20	v	x	Maltitol	x	x	D-Aspartic Acid	x	x
L-Rhamnose	x	x	a-Methyl-D-Galactoside	x	x	D-Glutamic Acid	v	v
D-Fructose	v	v	b-Methyl-D-Galactoside	x	x	D-Lysine	v	v
Acetic Acid	v	v	3-Methyl Glucose	x	x	D-Serine	v	v
D-(+)-Glucose	v	v	b-Methyl-D-Glucuronic Acid	x	x	D-Valine	v	v
Maltose	x	x	a-Methyl-D-Mannoside	x	x	L-Citrulline	v	v
D-Melibiose	x	x	b-Methyl-D-Xyloside	x	x	L-Homoserine	x	x
Thymidine	x	x	Palatinose	x	x	L-Ornithine	v	v
L-Asparagine	v	v	D-Raffinose	x	x	N-Acetyl-L-Glutamic Acid	v	v
D-Aspartic Acid	x	x	Salicin	x	x	N-Phthaloyl-L-Glutamic Acid	v	x
D-Glucosaminic Acid	x	x	Sedoheptulosan	x	x	L-Pyroglutamic Acid	v	v
1,2-Propanediol	v	v	L-Sorbose	x	x	Hydroxylamine	x	v
Tween 40	v	x	Stachyose	x	x	Methylamine	x	x
a-Keto-Gutaric Acid	v	v	D-Tagatose	x	x	N-Amylamine	x	x
a-Ketobutyric Acid	v	v	Turanose	x	x	N-Butylamine	x	x
a-Methyl-D-Galactoside	x	x	Xylitol	x	x	Ethylamine	x	x
a-D-Lactose	x	x	N-Acetyl-D-glucosaminitol	x	x	Ethanolamine	v	x
Lactulose	x	x	g-Amino Butyric Acid	v	v	Ethylenediamine	x	x
Sucrose	x	x	d-Amino Valeric Acid	v	v	Putrescine	v	v
Uridine	x	v	Butyric Acid	v	v	Agmatine	v	v
L-Glutamine	v	v	Capric Acid	x	v	Histamine	v	v
m-Tartaric Acid	x	x	Caproic Acid	v	v	b-Phenylethylamine	v	v
D-Glucose-1-Phosphate	x	v	Citraconic Acid	x	x	Tyramine	v	v
D-Fructose-6-Phosphate	x	x	Citramalic Acid	v	v	Acetamide	v	v
Tween 80	v	x	D-Glucosamine	x	x	Formamide	x	x
a-Hydroxy Glutaric Acid-g-Lactone	x	x	2-Hydroxybenzoic acid	x	x	Glucuronamide	v	v
D,L-a-Hydroxy-Butyric Acid	v	v	4-Hydroxy Benzoic Acid Sodium	v	v	D,L-Lactamide	v	v
b-Methyl-D-Glucoside	x	x	b-Hydroxy Butyric Acid	v	v	D-Glucosamine	x	x
Adonitol	x	x	g-Hydroxy Butyric Acid	x	v	D-Galactosamine	x	x
Maltotriose	x	x	2-Oxovaleric acid	x	x	D-Mannosamine	x	x
2'-Deoxy Adenosine	x	x	Itaconic Acid	v	v	N-Acetyl-D-Glucosamine	v	v
Adenosine	v	v	5-Keto-D-Gluconic Acid	x	x	N-Acetyl-D-Galactosamine	v	v
Glycyl-L-Aspartic Acid	x	v	D-Lactic Acid Methyl Ester	x	x	N-Acetyl-D-Mannosamine	x	x
Citric Acid	v	v	Malonic Acid	v	v	Adenine	v	v
m-Inositol	x	x	Melibionic Acid	x	x	Adenosine	v	v
D-Threonine	x	x	Oxalic Acid	x	x	Cytidine	v	v
Fumaric Acid	v	v	Oxalomalic Acid	x	x	Cytosine	v	v
Bromo Succinic Acid	v	x	Quinic Acid	v	v	Guanine	v	v
Propionic Acid	v	v	D-Ribono-1,4-Lactone	x	x	Guanosine	v	v
Mucic Acid	x	x	Sebacic Acid	x	x	Thymine	v	v
Glycolic Acid	x	x	Sorbic acid	v	v	Thymidine	x	x
Glyoxylic Acid	x	x	Succinamic Acid	v	v	Uracil	v	v
D-Cellobiose	x	x	D-Tartaric Acid	x	x	Uridine	v	v
Inosine	v	v	L-Tartaric Acid	x	x	Inosine	v	v
Glycyl-L-Glutamic Acid	x	v	Acetamide	x	v	Xanthine	v	v
Tricarballic Acid	x	x	L-Alaninamide	v	v	Xanthosine	v	v
L-Serine	v	v	N-Acetyl-L-Glutamic Acid	v	v	Uric Acid	v	v
L-Threonine	x	v	L-Arginine	v	v	Alloxan	v	x
L-Alanine	v	v	Glycine	v	v	Allantoin	v	v
Ala-Gly	x	v	L-Histidine	v	v	Parabanic Acid	v	x
Acetoacetic Acid	v	v	L-Homoserine	x	v	D,L-a-Amino-N-Butyric Acid	x	x
N-Acetyl-D-Mannosamine	x	x	Hydroxy-L-Proline	v	v	g-Amino Butyric Acid	v	v
Mono Methyl Succinate	v	v	L-Isoleucine	v	v	e-Amino-N-Caproic Acid	x	x
Methyl Pyruvate	v	x	L-Leucine	v	v	D,L-a-Amino- Caprylic Acid	x	x
D-Malic Acid	x	x	L-Lysine	x	v	d-Amino-N-Valeric Acid	v	v
L-Malic Acid	v	v	L-Methionine	x	v	a-Amino-N-Valeric Acid	v	x
Glycyl-L-Proline	v	v	L-Ornithine	v	v	Ala-Asp	v	v
p-Hydroxy Phenyl Acetic Acid	v	v	L-Phenylalanine	x	v	Ala-Gln	v	v
M-Hydroxy Phenyl Acetic Acid	x	x	L-Pyroglutamic Acid	v	v	Ala-Glu	v	v
Tyramine	v	v	L-Valine	x	v	Ala-Gly	v	v
D-Psicose	x	x	D,L-Carnitine	v	v	Ala-His	v	v
L-Lyxose	x	x	Sec-Butylamine	x	x	Ala-Leu	v	v
Glucuronamide	x	x	D,L-Octopamine	v	v	Ala-Thr	v	v
Pyruvic Acid	v	v	Putrescine	v	v	Gly-Asn	v	v
L-Galactonic Acid-g-Lactone	x	x	Dihydroxy Acetone	x	x	Gly-Gln	v	v
D-Galacturonic Acid	x	x	2,3-Butanediol	v	v	Gly-Glu	v	v
b-Phenylethylamine	x	x	Diacetyl	x	x	Gly-Met	x	v
2-Aminoethanol	v	v	3-Hydroxy 2-Butanone	x	x	Met-Ala	v	v




A**B**

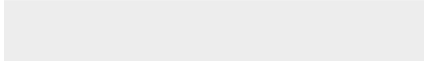
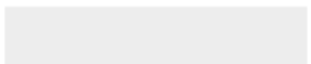


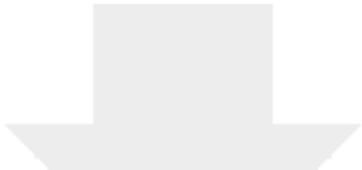
Click here to access/download
Supplementary Material
additionalFile1.docx






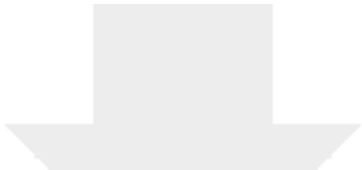
Click here to access/download
Supplementary Material
additionalFile2.xlsx







Click here to access/download
Supplementary Material
additionalFile3.xlsx



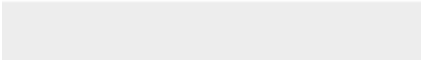



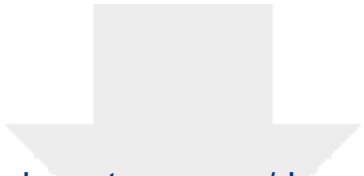
Click here to access/download
Supplementary Material
additionalFile4.xlsx






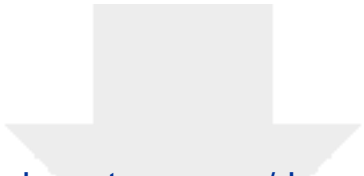
Click here to access/download
Supplementary Material
additionalFile5.xlsx






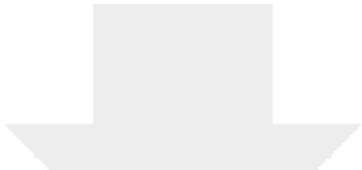
Click here to access/download
Supplementary Material
additionalFile6.xlsx






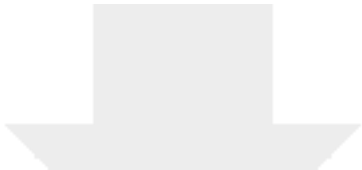
Click here to access/download
Supplementary Material
additionalFile7.xlsx






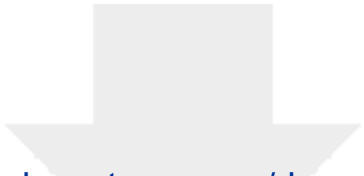
Click here to access/download
Supplementary Material
additionalFile8.xlsx






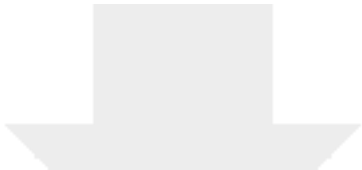
Click here to access/download
Supplementary Material
additionalFile9.xlsx






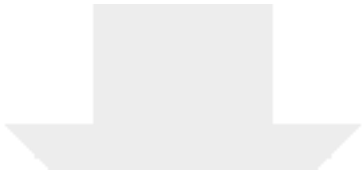
Click here to access/download
Supplementary Material
additionalFile10.xlsx






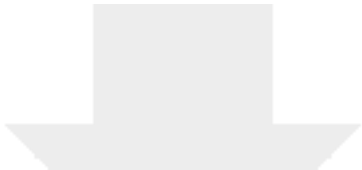
Click here to access/download
Supplementary Material
additionalFile11.xlsx






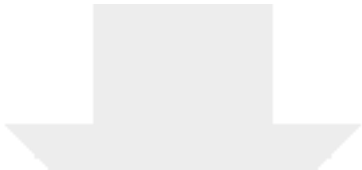
Click here to access/download
Supplementary Material
additionalFile12.xlsx






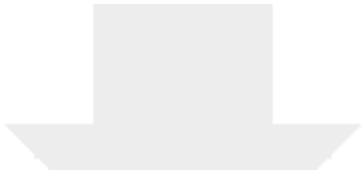
Click here to access/download
Supplementary Material
additionalFile13.xlsx






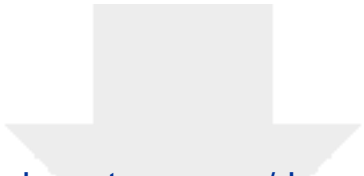
Click here to access/download
Supplementary Material
additionalFile14.xlsx







Click here to access/download
Supplementary Material
additionalFile15.xlsx



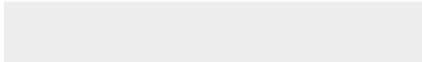




Click here to access/download
Supplementary Material
additionalFile16.xlsx



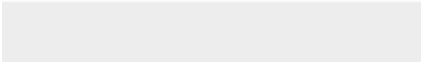



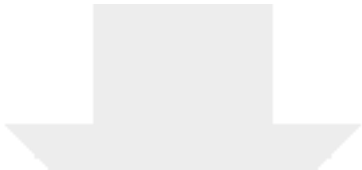
Click here to access/download
Supplementary Material
additionalFile17.xlsx






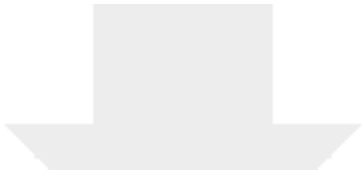
Click here to access/download
Supplementary Material
additionalFile18.xlsx






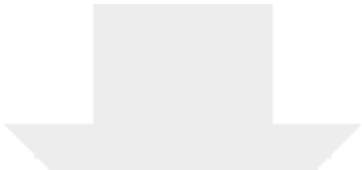
Click here to access/download
Supplementary Material
additionalFile19.xlsx






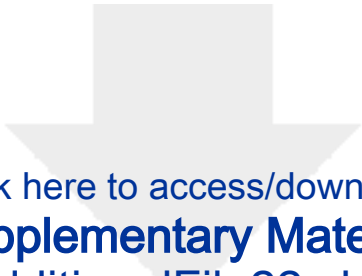
Click here to access/download
Supplementary Material
additionalFile20.xlsx



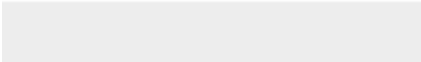



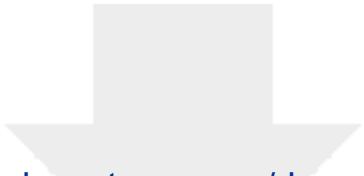
Click here to access/download
Supplementary Material
additionalFile21.xlsx






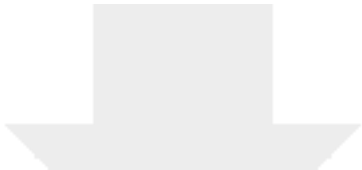
Click here to access/download
Supplementary Material
additionalFile22.xlsx






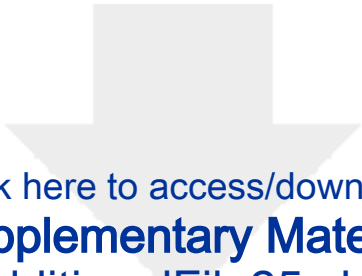
Click here to access/download
Supplementary Material
additionalFile23.xlsx



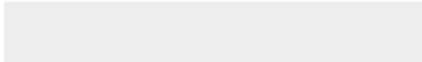



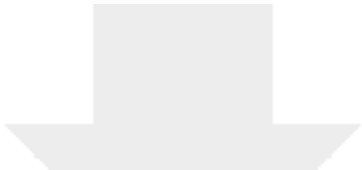
Click here to access/download
Supplementary Material
additionalFile24.xlsx







Click here to access/download
Supplementary Material
additionalFile25.xlsx



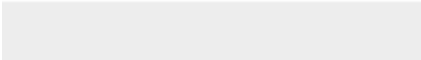



Click here to access/download
Supplementary Material
additionalFile26.xlsx





Click here to access/download
Supplementary Material
additionalFile27.xlsx





Professor Jian Li
Head, Laboratory of Antimicrobial Systems Pharmacology
Monash Biomedicine Discovery Institute

Dr Laurie Goodman
Editor-in-Chief
GigaScience

16 October 2017

Dear Dr Goodman,

We are pleased to submit our manuscript entitled “*Genome-scale metabolic modelling of responses to polymyxins in Pseudomonas aeruginosa*” for your consideration as an original Research Article in *GigaScience*.

Antimicrobial resistance has become one of the greatest threats to global health today. Multidrug-resistant (MDR) *P. aeruginosa* has been categorised by the World Health Organization as a “Critical” Gram-negative ‘superbug’ against which no new antibiotics will be available in the near future. Polymyxins are ‘old’ antibiotics firstly discovered in 1947, but have been abandoned since the 1970s. Over the last decade polymyxins have been revived as the last-line therapy against Gram-negative ‘superbugs’, including *P. aeruginosa*, which are resistant to all other antibiotics. However, the mechanism of their antibacterial activity remains largely unknown.

Here we report the construction of a superior genome-scale metabolic model (GSMM) *iPAO1* for *P. aeruginosa* PAO1 which represents *the largest genome-scale metabolic model thus far for any Gram-negative bacteria*. *iPAO1* provides a powerful systems pharmacology tool to elucidate the complex mode of action of antibiotics and shift the paradigm of the “one-gene, one-receptor, one-mechanism” approach. It is able to quantitatively simulate complex bacterial cellular responses in response to antibiotic treatments.

To date, there are four curated GSMMs for *P. aeruginosa*, iMO1056 (developed in 2008), Opt20896429 (2010), iMO1086 and iPae1146 (two minor updated versions of iMO1056 developed in 2011 and 2017, respectively), and all are for the strain PAO1. *Unfortunately, none of these four GSMMs incorporates the periplasmic space, and glycerolphospholipid (GPL) and lipopolysaccharide (LPS) biosynthesis is very poorly represented*. These shortcomings significantly limit their usefulness for antimicrobial pharmacology. Growth prediction with *iPAO1* on 190 carbon and 95 nitrogen nutrients outperformed all the previous models with an accuracy of 89.1%. Prediction of the essential genes for growth on rich media achieved a high accuracy of 87.9%. Specifically, the significant advantages of our *iPAO1* include: (1) incorporation of the periplasmic space; (2) addition of detailed GPL and LPS biosynthesis pathways supported by our own metabolomics and lipidomics data; and (3) significant expansion of the modelling scale with a high prediction accuracy. For the first time, metabolic simulation using *iPAO1* showed that lipid A modifications exert limited impacts on bacterial growth and metabolism, but remarkably change the physicochemical properties of bacterial outer membrane. Modelling with transcriptomics constraints revealed a broad range of metabolic responses to polymyxin treatment, including reduced biomass formation, upregulated amino acids catabolism, induced tricarboxylic acid cycle, and increased redox turnover. Overall,

Department of Microbiology
19 Innovation Walk
Monash University
VIC 3800, Australia
Telephone: (+61 3) 990 39702 Facsimile: (+61 3) 990 29222 Email: Jian.Li@monash.edu
Web: www.monash.edu/pharm/research/areas/drug-delivery/labs/li-lab

Unintended recipient: please notify as soon as possible and destroy all pages received



Professor Jian Li
Head, Laboratory of Antimicrobial Systems Pharmacology
Monash Biomedicine Discovery Institute

our GSMM approach has a significant potential in accelerating antimicrobial pharmacological discovery against Gram-negative 'superbugs'.

To the best of our knowledge, this study is the first to integrate antimicrobial pharmacology, computational biology, metabolic network and systems pharmacology to analyse large-scale datasets, in order to better understand the dynamic and complex nature of polymyxin killing and resistance. We believe this manuscript perfectly matches the theme of *GigaScience* and will be of broad interest to microbiologists, bioinformaticians and antimicrobial researchers.

We confirm that our submission comprises original and unpublished material which is not currently under consideration for publication elsewhere, and has been approved by all authors. Thank you for considering our work for publication in *GigaScience*. We look forward to your correspondence.

Yours sincerely,

A handwritten signature in blue ink, appearing to be 'Jian Li'.

Jian Li PhD

A handwritten signature in blue ink, appearing to be 'Falk Schreiber'.

Falk Schreiber PhD